J. Fluid Mech. (1994), *vol.* 262, *pp.* 75–110

Active turbulence control for drag reduction in wall-bounded flows

By HAECHEON CHOI, PARVIZ MOIN AND JOHN KIM†

Center for Turbulence Research, Stanford University, Stanford, CA 94305, USA *and* NASA Ames Research Center, Moffett Field, CA 94035, USA

(Received 3 March 1993 and in revised form 25 August 1993)

The objective of this study is to explore concepts for active control of turbulent boundary layers leading to skin-friction reduction using the direct numerical simulation technique. Significant drag reduction is achieved when the surface boundary condition is modified to suppress the dynamically significant coherent structures present in the wall region. The drag reduction is accompanied by significant reduction in the intensity of the wall-layer structures and reductions in the magnitude of Reynolds shear stress throughout the flow. The apparent outward shift of turbulence statistics in the controlled flows indicates a displaced virtual origin of the boundary layer and a thickened sublayer. Time sequences of the flow fields show that there are essentially two drag-reduction mechanisms. Firstly, within a short time after the control is applied, drag is reduced mainly by deterring the sweep motion without modifying the primary streamwise vortices above the wall. Consequently, the high-shear-rate regions on the wall are moved to the interior of the channel by the control schemes. Secondly, the active control changes the evolution of the wall vorticity layer by stabilizing and preventing lifting of the spanwise vorticity near the wall, which may suppress a source of new streamwise vortices above the wall.

1. Introduction

The potential benefits of controlling turbulent flows that occur in various engineering applications are known to be significant. Organized structures in turbulent flows play an important role in turbulent transport (Cantwell 1981; Robinson 1991). Therefore, attempts to control turbulent flows for engineering applications have focused on the manipulation of the coherent structures. Most turbulence control strategies have been developed for free-shear flows where the hydrodynamic stability mechanism in the near field is basically understood (Ho & Huang 1982). Turbulence control strategies to date for wall-bounded turbulent flows have focused on passive approaches. For example, devices such as riblets or LEBUs (large-eddy-break-up devices) may be placed in the boundary layer in an attempt to suppress the formation or interaction of organized flow structures. Such devices play a passive role in the sense that there exists no feedback loop to sense and then manipulate flow structures. The present study is aimed at the active control of dynamically significant coherent structures to achieve skin-friction reduction. The control strategy will respond through a feedback loop as flow structures are modified.

The most widely observed coherent structures in the wall layer are streaks: elongated

† Present address: Mechanical, Aerospace, and Nuclear Engineering Department, University of California, Los Angeles, CA 90024, USA.

regions of low- and high-speed fluid alternating in the spanwise direction. From flow visualization data, Kline *et al.* (1967) pointed out that the production of turbulence in boundary layers is largely due to the bursting event which consists of the lift-up, oscillation, and violent breakup of the streaks. The sweep event (Corino & Brodkey, 1969), which is described as the inrush of high-speed fluid towards the wall, is also believed to be a major contributor to turbulence production. Some of these event-oriented descriptions of important phenomena in turbulent boundary layers are beginning to change, largely from examination of direct numerical simulation databases. For example, the bursting event appears to be a consequence of the convection of a single streamwise vortex past a fluid marker (Kim & Moin 1986). The passage of the vortex lifts the marker, and as the marker wraps around the vortex, it appears from a side view that the marker is oscillating on a vertical plane. In this paper, we use the terms *sweep* and *ejection* at a *point* to simply denote the flow direction towards or away from the wall respectively.

Contour plots of instantaneous turbulent velocity and pressure fluctuations show that only the contours of constant streamwise velocity component are significantly elongated in the streamwise direction. The pressure patterns are more rounded, and the normal (to the wall) velocity component is highly intermittent (Moin 1987). Therefore, intense regions of turbulence production are also highly intermittent. One of the most striking features of turbulent boundary layers are the strong shear layers protruding from the wall into the flow (Jiménez *et al.* 1988). Virtually every snap-shot of the flow in the form of a contour plot of the spanwise component of vorticity, ω_z, contains these shear layers. Moreover, their shape is very similar to those observed in transitional channel flow (Jiménez 1987). The shear layers are associated with high turbulence production and have long lifetimes, travelling in a straight path downstream (Johansson, Alfredsson & Kim 1987). In addition, both experimental and numerical data indicate that the shear layers have high-amplitude pressure signatures at the wall (Johansson, Her & Haritonidis 1987; Alfredsson, Johansson & Kim 1988), which is of particular interest for their detection in an active control experiment.

Direct numerical simulations have emerged as a powerful tool in turbulence structure research. Owing to the availability of all the flow variables at many spatial locations and the ability to readily alter flow boundary conditions, numerical simulations provide the means for testing and designing turbulence control concepts. Although some of the concepts may not turn out to be feasible for implementation in the foreseeable future, simulations can provide data on what may be possible to achieve just from fluid dynamical considerations. The primary role of simulations in the field of flow control will be to guide experiments for complex flows.

Computer simulations have been used for active stabilization of laminar boundary layers (Metcalfe *et al.* 1986). Laurien & Kleiser (1989) studied the control of laminar/turbulent transition by local two-dimensional suction and blowing at the wall and showed that transition was delayed or accelerated by superposing disturbances which were out of phase or in phase with incoming Tollmien–Schlichting waves, respectively. Early work on control of fully developed turbulent flows via numerical simulations has been limited to passive control (Kuhn *et al.* 1984).

In this paper, we use the direct numerical simulation technique to explore concepts for manipulation of turbulent channel flow with the ultimate goal of drag reduction. The base flow is fully developed turbulent channel flow (Kim, Moin & Moser 1987). A brief description of the numerical procedures used in this study is given in §2. In §3, several numerical experiments for active control of turbulent channel flow are described. Turbulence statistics of the manipulated channel flows are given in §4.

Modified turbulence structures and mechanisms of drag reduction by active manipulation at the wall are presented in §5, followed by a summary in §6.

2. Numerical procedures

The numerical technique used in this study is nearly the same as that of Kim *et al.* (1987), to which the reader is referred for a detailed description. The only difference is that the time advancement scheme for the convective terms was a third-order Runge–Kutta method instead of the original Adams–Bashforth method. The advantage of using a third-order Runge–Kutta method is that a larger computational time step can be used and there is no spurious root which is associated with multi-step methods. The boundary conditions for the wall velocity components are modified according to the particular control strategy.

The base flow is a fully developed channel flow. Fully developed turbulent channel flow is homogeneous in the streamwise and spanwise directions, and periodic boundary conditions are used in these directions. Most experiments were performed using $32 \times 65 \times 32$ spectral (streamwise, normal to the wall, and spanwise, respectively) at $Re_c = 1800$ based on the centreline velocity of the unmanipulated channel and the channel half-width. Starting with the same initial field, different boundary conditions were tested (§3). The most successful control strategies (v- and w-controls; see §3) were repeated using $128 \times 129 \times 128$ spectral modes at $Re_c = 3300$, from which most of results presented in §§4 and 5.1 were obtained. This particular Reynolds number was chosen for comparison with the results for the unmanipulated channel (Kim *et al.* 1987). For the Reynolds numbers considered here, the streamwise and spanwise computational periods (L_x and L_z) are chosen to be $4\pi\delta$ and $\frac{4}{3}\pi\delta$, respectively.

In this paper, x, y, and z denote the streamwise, normal to the wall, and spanwise directions, respectively. The velocities are u, v, and w in the x-, y-, and z-directions, respectively, and are used interchangeably with the subscripted variables u_1, u_2, and u_3. An overbar indicates an average over x and z, and a prime indicates perturbation from this average. The subscript w indicates the value at the wall, and the superscript + indicates a non-dimensional quantity scaled by the wall variables: for example, $y^+ = yu_\tau/\nu$, where ν is the kinematic viscosity and $u_\tau = (\tau_w/\rho)^{\frac{1}{2}}$ is the wall-shear velocity. The skin friction and the drag are used synonymously in this paper because there is no form drag in the flat channel flow.

3. Active control experiments

Several different control strategies were investigated for the purpose of drag reduction: controls with the normal, spanwise and streamwise velocities imposed at the wall; control with selective normal velocity; and control with the sensors limited to the wall. All numerical experiments were conducted in a fully developed channel flow. Unmanipulated channel flow provided a base for comparison. In the control experiments, all conditions were kept the same as in the unmanipulated simulation except for the boundary conditions through which control strategies were implemented. The skin-friction reduction was measured in terms of the change in the mean pressure gradient necessary to drive the flow with a fixed mass flow rate. Most of the computations were carried out with a coarse grid ($32 \times 65 \times 32$) at $Re_c = 1800$. The use of this coarse grid allowed the exploration of many different strategies for optimum control which would otherwise have required excessive computer resources. The results presented in this section were obtained for the Reynolds number of 1800. To validate

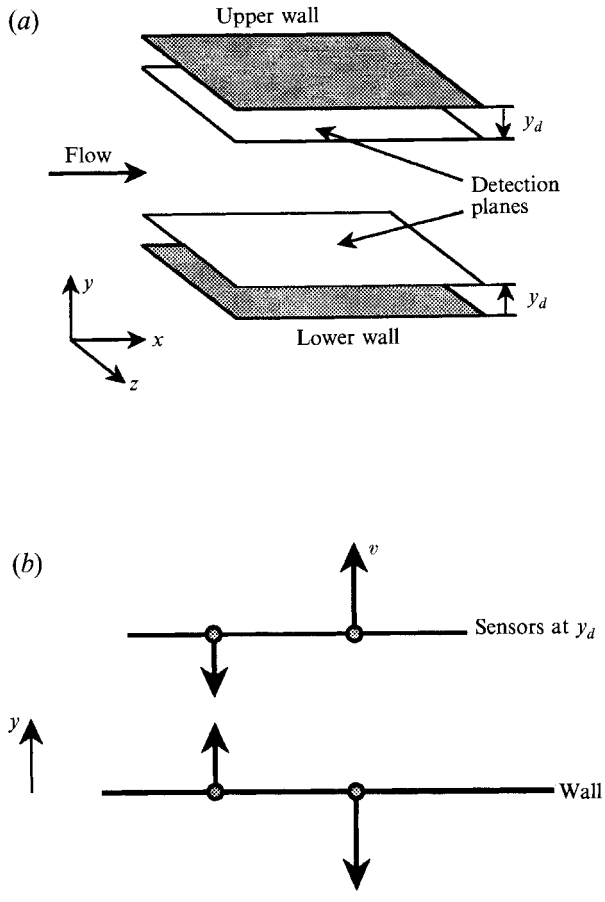

FIGURE 1. (*a*) Three-dimensional view of detection planes (*b*) schematic diagram of out-of-phase v-control.

the coarse-grid computations, some calculations were performed with a fine grid ($128 \times 129 \times 128$), yielding essentially the same results for low-order statistics.

Based on the knowledge that most of the Reynolds-stress-producing events are associated with streamwise vortices (Moin 1987; Robinson 1991), we explored several strategies with the aim of reducing the strength of the streamwise vortices. A summary of results obtained using different control strategies is presented in the following subsections.

3.1. *Control with the normal velocity* (*v-control*)

The aim of this study was to examine if we can reduce the wall skin friction by suppressing the sweep and ejection events. We applied blowing or suction on the channel walls exactly opposite to the normal component of the velocity at a prescribed y-location (see figure 1). At each instant the boundary condition for $v(x, z)$ at the wall was prescribed to be $-v(x, z)$ at y_d, where $y_d(> 0)$ is the distance of the detection point measured from the wall. Thus, when fluid moving toward the wall (sweep) was detected at y_d, an equally strong blowing velocity was imposed at the wall to 'cancel' the sweep event. Similarly, when fluid moving away from the wall (ejection) was detected at y_d, an equally strong suction was applied. The initial condition for the calculations was an instantaneous velocity field from the unmanipulated fully developed channel flow. The mass flux through the channel remained constant since the equation of continuity

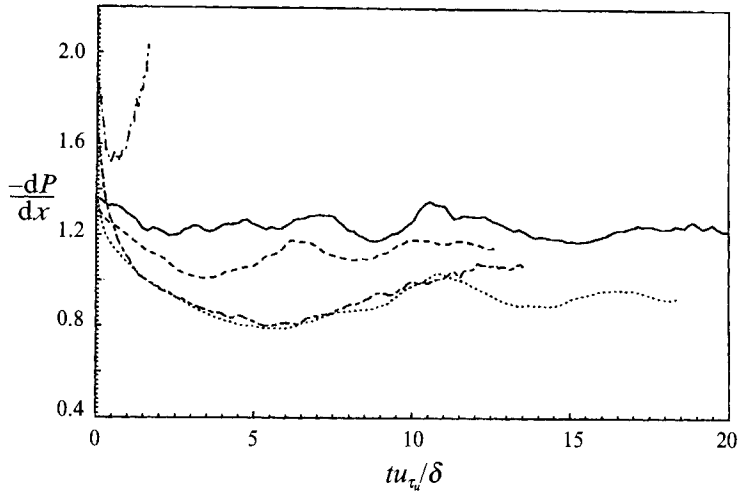

FIGURE 2. Time history of the pressure gradient required to drive a fixed mass flow rate in the case of v-control: —, unmanipulated channel; – – –, manipulated channel with sensors at $y_d^+ \approx 5$; · · · · · · · · ·, $y_d^+ \approx 10$; – – –, $y_d^+ \approx 20$; – · –, $y_d^+ \approx 26$.

implies $\int_{L_z}\int_{L_x} v(x, y, z)\, dx\, dz = 0$ for any y. Thus, any skin-friction reduction would be manifested in the change in the mean pressure gradient necessary to drive the flow with a fixed mass flow rate. Several computations were performed for different y_d to examine the effect of the detection location. Using the same initial velocity field, the calculations were continued with the new boundary conditions, until a new statistically steady state was obtained or until it became apparent that the drag would increase substantially.

Figure 2 shows the time histories of the pressure gradients that were required to drive a fixed mass flow rate for the unmanipulated fully developed channel flow and for manipulated channel flows. Substantial skin-friction reduction was obtained ($\approx 25\%$ on each wall) with $y_d^+ \approx 10$. For other y_d^+ locations, either the drag was substantially increased ($y_d^+ \approx 26$) or the reduction was small ($y_d^+ \approx 5$). Here, y_d^+ was defined with the unmanipulated wall-shear velocity, u_{τ_u}, at $t = 0$. Hence, a fixed y_d location was obtained using $y_d = \nu y_d^+/u_{\tau_u}$. Note that for the Reynolds number considered, $Re_c = 1800$, the maximum turbulent drag reduction possible is 63% (74% for $Re_c = 3300$), which would correspond to the flow becoming laminar. Apparently there is a critical value of y_d beyond which the flow becomes unstable with substantial drag increase.

The efficiency of the process was measured by estimating the ratio of the power saved $((-dP/dx|_u + dP/dx|_m)\, U_m)$ to the ideal power input $(p_w v + \frac{1}{2}\rho v^3)$, where $-dP/dx|_u$ and $-dP/dx|_m$ are the mean pressure gradients for the unmanipulated and manipulated channels, respectively, U_m is the bulk mean velocity. For the case of 25% reduction, the ratio was about 30, indicating that the required ideal power input was negligible. This estimate did not take into account, for example, the valve losses that would be present in practical applications. Finally, it should be pointed out that in-phase control, i.e. when $v(x, z)$ at the wall was prescribed to be $v(x, z)$ at y_d, led to a significant drag increase.

We also performed selective control experiments to affect only the strong events. The out-of-phase boundary condition was applied at the surface only when the normal velocity at the sensor location y_d exceeded at threshold value, v_{th}. In the comparison to the 25% reduction for $v_{th} = 0$, 20% and 15% reductions were obtained with

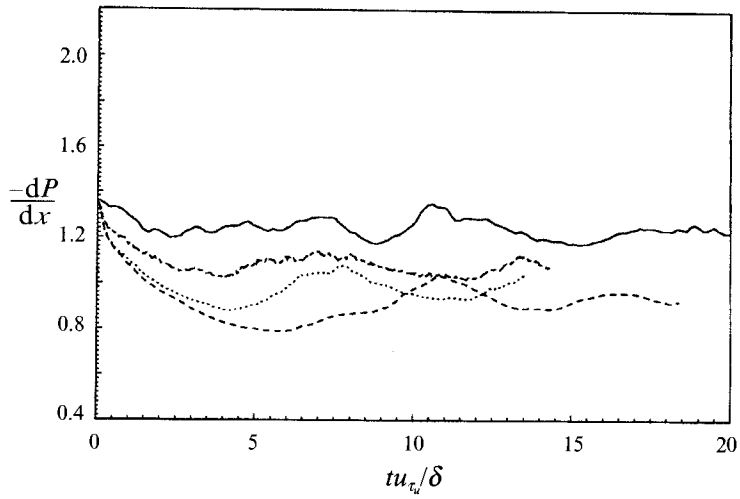

FIGURE 3. Time history of the pressure gradient required to drive a fixed mass flow rate: —, unmanipulated channel: – – –, minipulated channel at the sensor location $y_d^+ \approx 10$ exceeded a threshold value $v_{th} = 0$; · · · · · · · · ·, $v_{th} = v_{rms}$; – – –, $v_{th} = 2v_{rms}$.

$v_{th} = v_{rms}$ and $v_{th} = 2v_{rms}$, respectively (figure 3), where v_{rms} is the root-mean-square value of the normal velocity at $y = y_d$. Only 25% and 5%, respectively, of the total surface area are controlled, indicating that most of the reduction was indeed due to the suppression of the stronger events.

It is known that uniform blowing decreases skin friction and increases the strength of the fluctuating quantities, but uniform suction has nearly the opposite effect. To investigate which part of the control processes, i.e. blowing or suction, is more effective in achieving the skin-friction reduction, several combinations of blowing/suction strategies were investigated. In the active control simulations, blowing reduces the strength of the fluctuating quantities as well as the skin friction. The amount of the skin-friction by active blowing is larger than that by uniform blowing when the mean value of active blowing is the same as the magnitude of uniform blowing. Active suction increases the skin friction less than uniform suction does, but significantly stabilizes the flow.

Other numerical experiments, such as control of a selective bandwidth of the streamwise and spanwise wavelengths, control with sensor locations at a fixed y^+ instead of y, control applied to only a portion of the surface area, and control on only one channel wall, were conducted. Controls based on selective wavelengths were conducted to obtain the characteristic length-scales of the normal velocity signal above the wall which are closely related to the skin friction on the wall: the velocity $v(x, z)$ at y_d was Fourier-transformed, and selectively filtered to retain certain Fourier coefficients. The filtered signal was used as the boundary condition for the normal velocity. The most significant result among selective controls based on wavelengths was that up to 10% drag reduction was obtained by applying the control to only one streamwise Fourier coefficient corresponding to the largest wavelength ($k_x = 0.5$) and all the spanwise waves. Control with sensor locations at a fixed y^+ gave the same skin-friction reduction as control with a sensor location at a fixed y. In the case of fixed-y^+ control, the distance of the sensors from the wall moves in the normal direction, because the control changes the value of the mean wall-shear velocity. Control was also applied to only a portion of the surface area. Half and quarter stripped walls of the

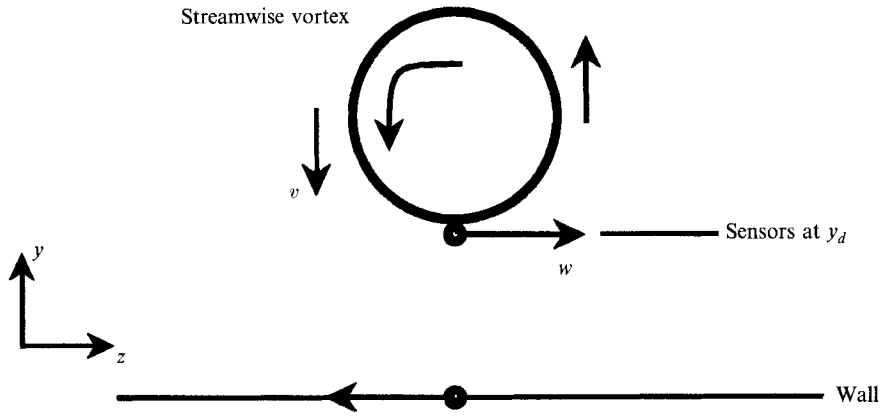

FIGURE 4. Schematic diagram of out-of-phase w-control.

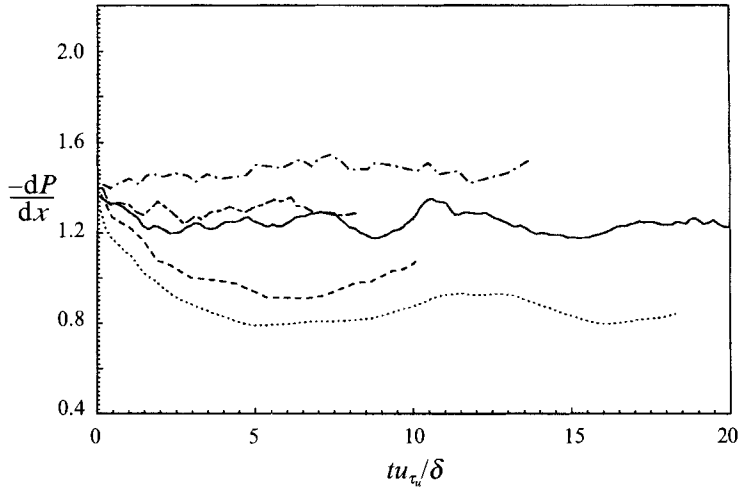

FIGURE 5. Time history of the pressure gradient required to drive a fixed mass flow rate in the case of w-control: —, unmanipulated channel; – – –, manipulated channel with sensors at $y_d^+ \approx 5$; · · · · · · · · ·, $y_d^+ \approx 10$; – – –, $y_d^+ \approx 20$; – · –, $y_d^+ \approx 26$.

channel were exposed to a control input velocity. Skin-fraction reduction was proportional to the surface area being controlled. In order to investigate whether the control at one wall affects the skin-friction at the other wall, control was applied to only one wall. The skin-friction reduction on the manipulated wall was identical to that obtained on one wall when control was applied at both walls, and the value of the skin friction on the unmanipulated wall was the same as that of the natural channel flow, indicating that there is virtually no communication between the two walls.

3.2. *Control with the spanwise velocity (w-control)*

Noting that streamwise vortices lead to strong spanwise velocity as well as normal velocity, the out-of-phase boundary condition was applied to the spanwise velocity at the surface (figure 4). Several sensor locations ranging from $y_d^+ \approx 5$ to 26 were tested, and the best result was obtained with $y_d^+ \approx 10$, yielding about 30% drag reduction (figure 5), slightly better than the optimum v-control. With $y_d^+ > 20$ the drag was increased. In-phase control of the spanwise velocity gave a significant increase of drag.

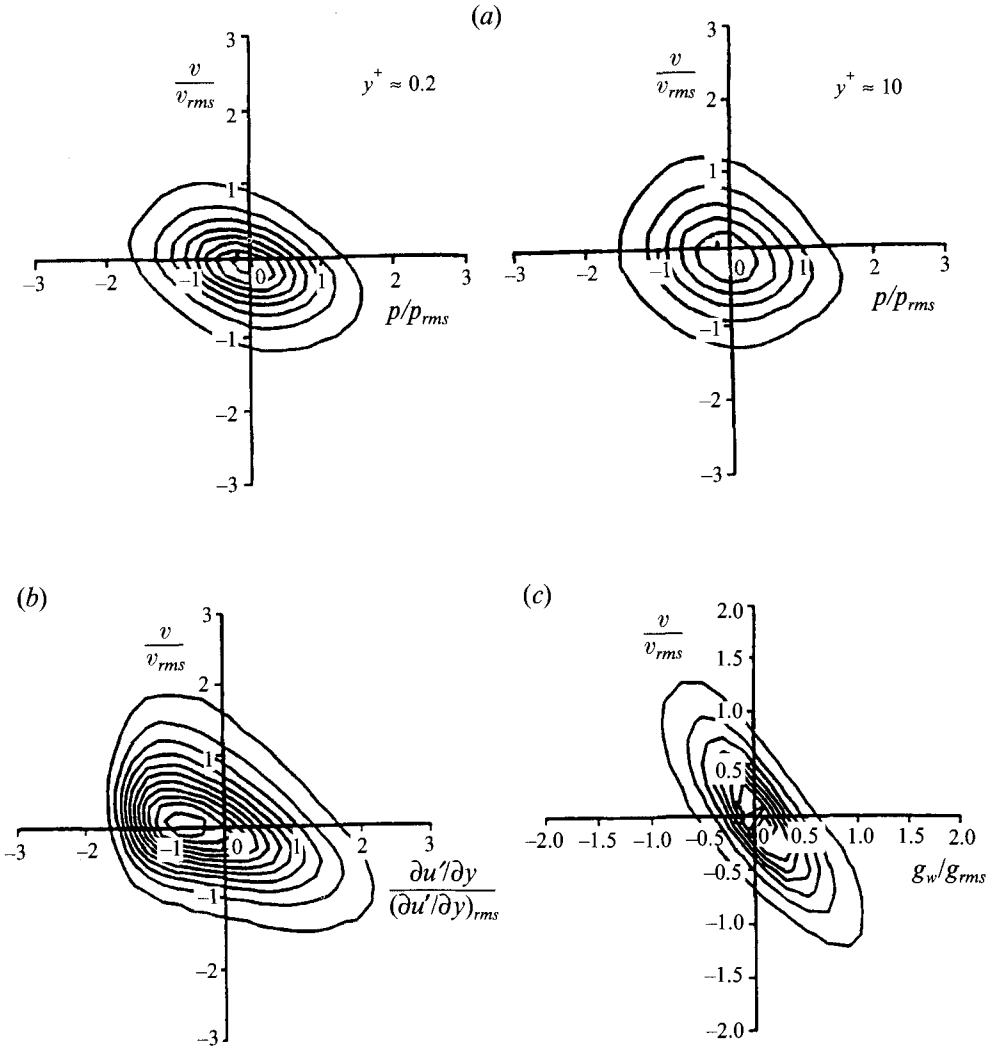

FIGURE 6. Joint probability density: (*a*) of the wall pressure fluctuations and the normal velocities at $y^+ \approx 0.2$ and $y^+ \approx 10$ (the value of the outer contour in each plot is 0.05, and the increment is 0.05); (*b*) of the fluctuating wall-shear rate and the normal velocity at $y^+ \approx 10$ (the contour levels are from 0.025 to 0.275 by increments of 0.025); (*c*) of g_w and the normal velocity at $y^+ \approx 10$ (the contour levels are from 0.125 to 0.875 by increments of 0.125).

3.3. *Combined control (v- and w-control)*

The out-of-phase boundary condition was applied to both v and w at the surface, which corresponds to blowing and suction with different angles to the wall. This combined control yielded 30% reduction which is nearly the same as in the w-control. In some cases, depending upon the initial field, the combined control was so effective that the flow became laminar. The laminarization is probably due to the low Reynolds number of the simulation (below the critical value) and probably would not occur at high Reynolds numbers.

3.4. *Control with the streamwise velocity (u′-control)*

Since the skin friction is directly related to the streamwise velocity near the wall, we could affect the drag by modifying the streamwise velocity near the wall through a 'u'-control' scheme. The out-of-phase u'-control with $y_d^+ \approx 10$ actually resulted in an increase, while the in-phase control (that is, the velocity at the surface has the same sign as that at the sensor location) gave about 10% reduction. This is an expected result since the in-phase control reduces $\partial u'/\partial y$ at the wall while the out-of-phase control increases the streamwise velocity gradient at the wall. However, it is rather surprising that we cannot do better than 10% reduction with u'-control while up to 30% drag reduction was achieved with transverse velocity controls.

3.5. *Control with the sensors at the wall*

Although the control algorithms described above were successful in reducing the drag, they are not feasible for practical implementation. Among other things, it is not practical to place sensors within the flow field. We therefore investigated the possibility of using flow variables at the wall for detection of structures above the wall. The objective was to determine the extent to which one can reproduce the v-control experiment by placing sensors only *at* the wall.

Joint probability density functions were used to examine the relationship between the wall variables and the flow above the wall. Three different wall variables – wall pressure, streamwise wall-velocity gradient $\partial u'/\partial y|_w$, and a quantity derived from the Taylor series expansion of the normal velocity component about the wall – were examined.

The joint probability density functions of the wall pressure and the normal velocity at different y-locations did not reveal any particular correlations (figure 6*a*), indicating that wall pressure alone is not an adequate detector of the flow toward the wall or away from it. One may wonder whether the downstream wall pressure is more appropriate to detect the normal velocity above the wall because the representative flow pattern around high-pressure fluctuations at the wall is that of upstream inrush of high-speed fluid impinging on the wall followed by the ejection of low-speed fluid downstream (Moin, Kim & Choi 1989). However, the joint probability density function of the wall pressure and the upstream normal velocity showed only a little improvement in the correlation.

The joint probability density function of $v(y^+ \approx 10)$ and $\partial u'/\partial y|_w$ is shown in figure 6(*b*). The streamwise velocity derivative at the wall appears to be a better detector of the events at $y^+ \approx 10$ than the pressure; in particular, high-amplitude positive values of $\partial u'/\partial y|_w$ are likely to be associated with sweeps. Negative values of $\partial u'/\partial y|_w$, however, do not provide adequate discrimination between sweeps and ejections.

The leading term in the Taylor series expansion of v near the wall is

$$v(y) = \frac{y^2}{2}\frac{\partial^2 v}{\partial y^2}\bigg|_w + \ldots.$$

From the continuity equation, one can deduce the equivalent relationship

$$v(y) = -\frac{y^2}{2}\left[\frac{\partial}{\partial x}\frac{\partial u}{\partial y}\bigg|_w + \frac{\partial}{\partial z}\frac{\partial w}{\partial y}\bigg|_w\right] + \ldots.$$

Our numerical tests have shown that the correlation of the first term in the bracket

with $v(y^+ \approx 10)$ is negligible. The joint probability density of v at $y^+ = 10$ and $g_w = (\partial/\partial z)/\partial w/\partial y|_w$ (figure 6*c*) indicates a high correlation between the two variables, suggesting that g_w could be a good candidate for the surface detection criterion.

A v-control experiment based on g_w yielded only about 6% reduction of drag. For the w-control experiments, we used $\partial w/\partial y|_w$ as the detection criterion, because it is a first leading-order term in the Taylor series expansion of the spanwise velocity component about the wall, and obtained essentially the same result. These results were rather disappointing considering that passive control of turbulence with surface riblets can yield about the same drag reduction (Walsh 1982; Choi, Moin & Kim 1993).

4. Turbulence statistics of the manipulated channel flows

Some key features of the flow fields obtained using v- and w-control schemes were studied to examine the differences between manipulated and unmanipulated channel flows. For detailed analysis of the modified flow fields, we performed fine-mesh computations for the optimum case of $y_d^+ \approx 10$, using $128 \times 129 \times 128$ spectral modes for $Re_c = 3300$ based on the centreline velocity of the unmanipulated channel and the channel half-width.

The statistically steady states of the manipulated channel flows were identified by the linear profile of total shear stress, $-\overline{u'v'} + (1/Re_c)\partial\bar{u}/\partial y$, and by quasi-periodic behaviour of the horizontally averaged wall-shear rate. Statistics reported here were averaged only over planes parallel to the wall. Therefore, some statistical fluctuations are expected to be present.

The statistics of the manipulation channel flows were compared to those of the unmanipulated channel flow (Kim *et al.* 1987). All velocity and length scales are normalized by either the unmanipulated wall-shear velocity u_{τ_u}, or the *actual* wall-shear velocity u_τ and the channel half-width δ, where the *actual* wall-shear velocity u_τ is the same as u_{τ_u} for the unmanipulated channel and u_{τ_m} for the manipulated channel. The wall coordinate y^+ was obtained using the actual wall-shear velocity u_τ unless otherwise indicated. The Reynolds number based on the actual wall-shear velocity u_τ and channel half-width δ is about 155 for the manipulated channel flows, and 180 for the channel flow. The Reynolds number based on the bulk mean velocity and the channel width is constant ($Re_m \approx 5600$) regardless of the control because the mass flow rate is kept constant through the computations.

4.1. *Mean properties*

The mean-velocity profiles normalized by the actual wall-shear velocities are shown in figure 7 for both unmanipulated and manipulated channels. The mean velocity profiles in v- and w- control channels are nearly the same. The slope of the long-law in the manipulated channels remains about the same as that in the unmanipulated channel. However, the intercept of the log-law with $u^+ = y^+$ was increased from $y^+ \approx 10$ in the unmanipulated channel to $y^+ \approx 15$. This upward shift in the log-law has previously been observed in drag-reduced flows such as large-eddy breakup devices (Bandyopadhyay 1986; Nguyen, Savill & Westphal 1987), riblets (Walsh 1982; Hooshmand *et al.* 1983; Choi 1989; Choi *et al.* 1993), and polymers (Lumley 1973; Virk 1975).

The shift in the log-law may be considered to be a result of the increase of the viscous sublayer thickness. From the Taylor series expansion,

$$\bar{u}(y) = \left.\frac{\partial\bar{u}}{\partial y}\right|_w y + \frac{1}{2}\left.\frac{\partial^2\bar{u}}{\partial y^2}\right|_w y^2 + O(y^3).$$

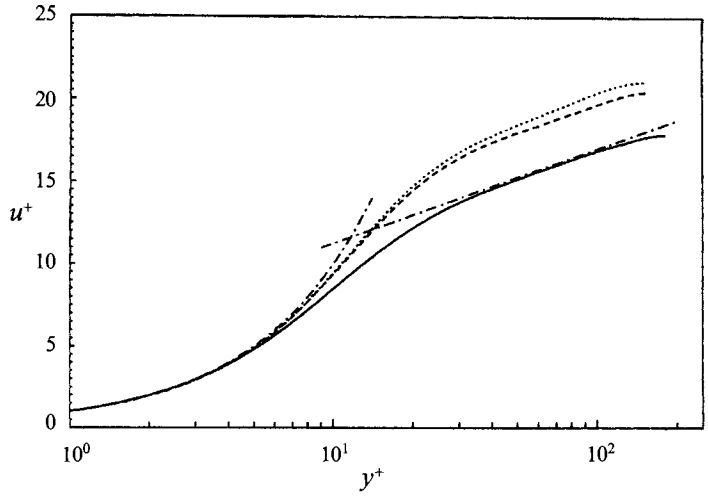

FIGURE 7. Mean-velocity profiles: —, no control; – – –, v-control; · · · · · · · · ·, w-control; –·–, law of the wall ($u^+ = y^+$ and $u^+ = 2.5 \ln y^+ + 5.5$).

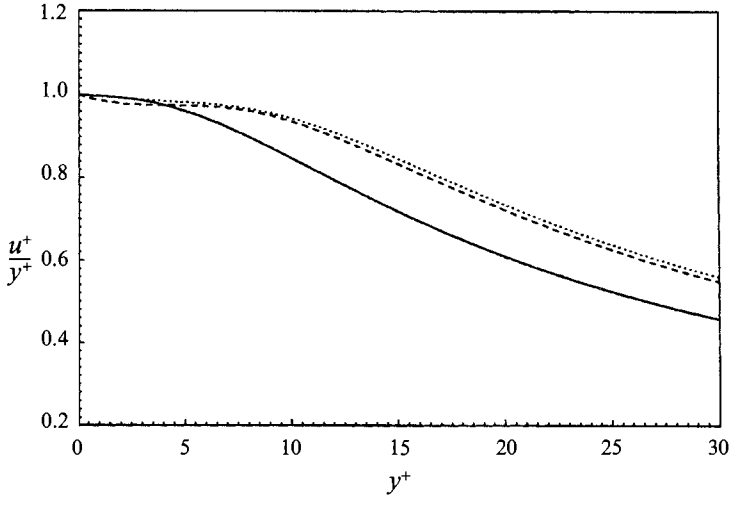

FIGURE 8. Near-wall behaviour of the mean velocity: —, no control; – – –, v-control; · · · · · · · · ·, w-control.

Case	Re_m	Re_c	Re_τ	u_τ/U_m	U_c/U_m	C_f	δ^*/δ	θ/δ
No control	5600	3300	180	0.064	1.16	8.37×10^{-3}	0.135	0.083
v-control	5600	3300	158	0.057	1.16	6.40×10^{-3}	0.137	0.079
w-control	5600	3300	154	0.055	1.16	6.09×10^{-3}	0.140	0.080

TABLE 1. Mean flow variables of the manipulated and unmanipulated channel flows. The bulk mean velocity is defined as $U_m = \frac{1}{2}\int_{-1}^{1} \bar{u}\, \mathrm{d}(y/\delta)$; and $C_f = \tau_w/\frac{1}{2}\rho U_m^2$.

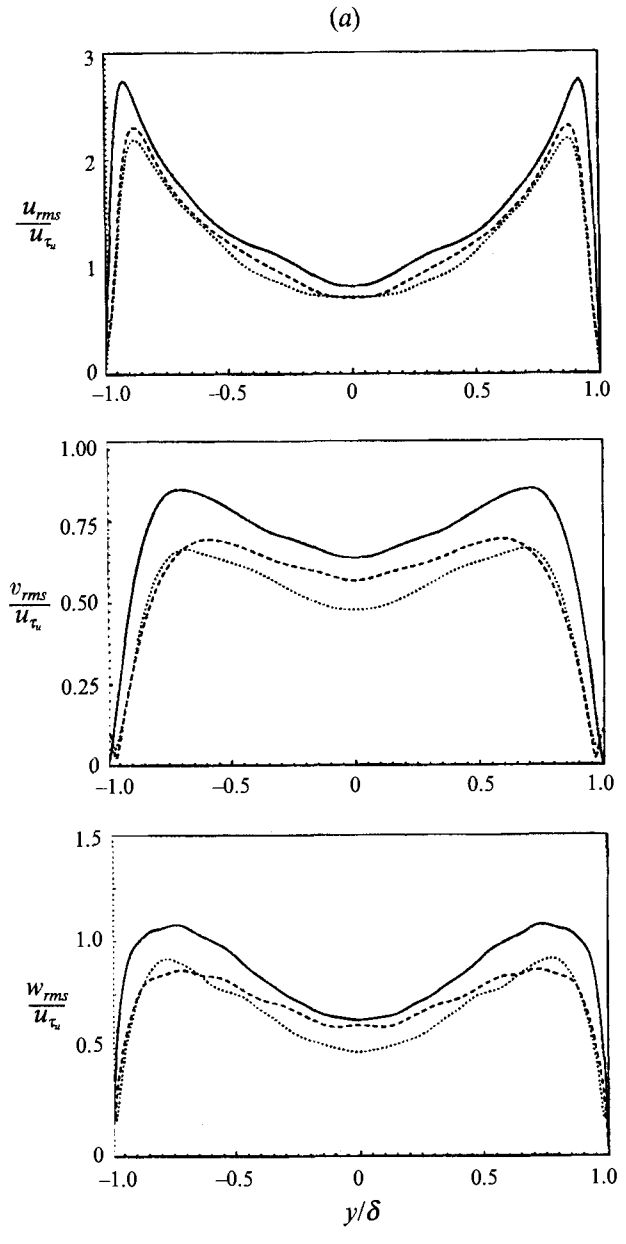

FIGURE 9(*a*). For caption see facing page.

Using the streamwise momentum equation and $\partial u/\partial x = \partial u/\partial z = 0$ at the wall, the above equation can be recast in terms of wall variables as follows:

$$u^+ = y^+ - \frac{1}{2Re_\tau}\left(\frac{\delta}{u_\tau^2}\right)\left[-\frac{1}{\rho}\frac{\mathrm{d}P}{\mathrm{d}x} - \overline{v_w \frac{\partial u'}{\partial y}\bigg|_w}\right] y^{+^2} + O(y^{+^3}),$$

where $u^+ = \bar{u}/u_\tau$, $y^+ = u_\tau y/\nu$, $Re_\tau = u_\tau \delta/\nu$, and $-\mathrm{d}P/\mathrm{d}x(>0)$ is the mean pressure gradient. In the case of the unmanipulated channel flow ($v_w = 0$), the departure from $u^+ = y^+$ is mainly due to the mean pressure gradient. As shown in figure 6 (*b*), the correlation between v_w ($= -v$ at $y^+ \approx 10$) and $\partial u'/\partial y|_w$ is relatively weak; therefore, the

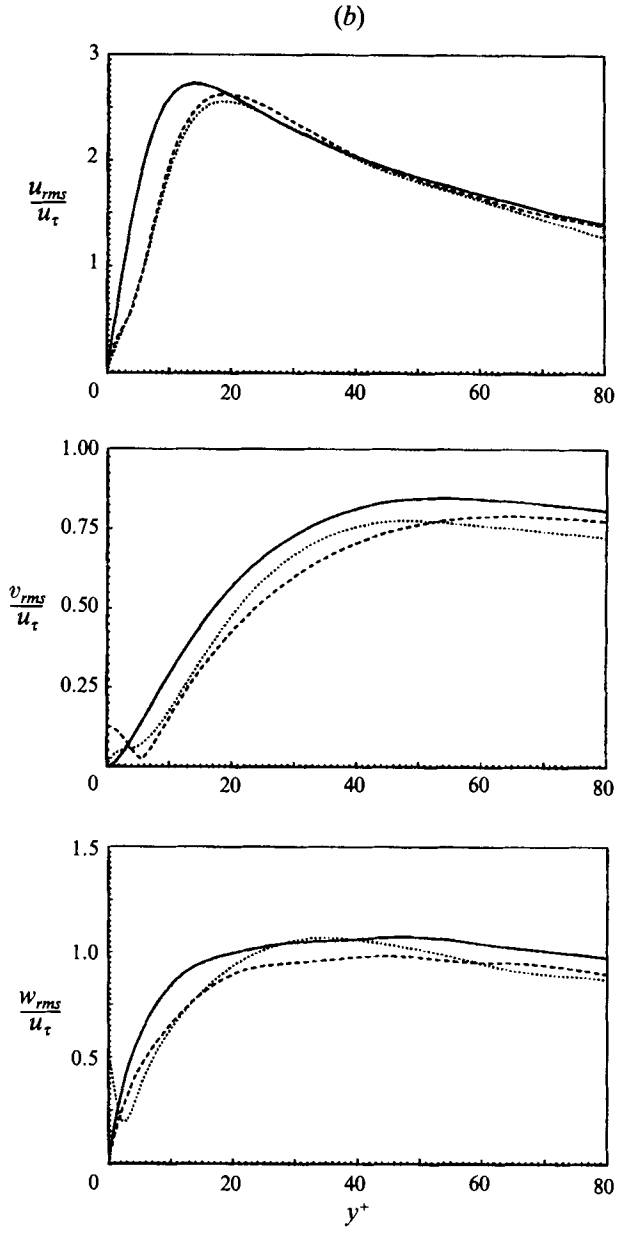

FIGURE 9. Root-mean-square fluctuations normalized by the wall-shear velocity; —, no control; – – –, v-control; · · · · · · · · ·, w-control. (*a*) In global coordinates; (*b*) in wall coordinates. Note that in wall coordinates, u_τ is u_{τ_u} for the unmanipulated wall and u_{τ_m} for the manipulated wall, and $y^+ = yu_\tau.\nu$.

magnitude of $\overline{v_w \partial u'/\partial y|_w}$ is much smaller than that of the mean pressure gradient in the case of v-control. In the case of w-control ($v_w = 0$), $\overline{v_w \partial u'/\partial y|_w} = 0$. Thus, again the departure from $u^+ = y^+$ is mainly due to the mean pressure gradient. The reduction of the coefficient of y^{+^2} is accompanied by the drag (or mean pressure gradient) reduction as a result of the control. Figure 8 shows the limiting behaviour of the mean velocities. The viscous sublayer thickness y_s^+, in which $u^+/y^+ \approx 1$ is satisfied, is increased by the

control. For the unmanipulated channel, $y_s^+ \approx 5$; for the manipulated channels, $y_s^+ \approx 10$ (these y_s^+ values were chosen using the criterion $u^+/y^+ > 0.95$ in figure 8).

Other mean properties, such as the skin-friction coefficient, displacement thickness, and momentum thickness, are shown in table 1. Comparison of these properties with experimental data is documented in Kim *et al.* (1987) for the manipulated channel flow. A reduction in the skin-friction coefficient C_f in the controlled cases is evident from table 1. The boundary-layer thickness in wall in wall units, $\delta^+ = Re_\tau$, is also reduced due to the skin-friction reduction. The displacement thickness δ^* is slightly increased, while the momentum thickness θ is slightly decreased. For the case of flat-plate boundary-layer flows, the momentum thickness is directly related to the skin friction at the wall, so that a decrease of the momentum thickness correlates with a reduction in skin friction (White 1974).

4.2. *Turbulence intensities*

Turbulence intensities in the manipulated channels are shown in figure 9, and they are compared with those above the unmanipulated wall (Kim *et al.* 1987). Turbulence intensities are significantly reduced by the control throughout the channel. The increase of v_{rms} or w_{rms} very near the wall is due to the input control. The changes of turbulence intensities with the active control schemes are in sharp contrast to the results of Kuhn *et al.* (1984) using a compliant surface and Choi (1989) using a longitudinal riblet, in which only local modification in the near-wall region was observed. Normalization of the turbulence intensities and the distance from the wall with the actual wall-shear velocity u_τ is shown in figure 9(*b*). The major difference among the data sets is the apparent outward shift of the controlled data, suggesting a displaced virtual origin of the boundary layer and a thickened sublayer. The value of the outward shift of the turbulence intensities is approximately 5 wall units, which coincides with the increased viscous-sublayer thickness. The structural change of turbulence near the wall will be discussed in detail in §5.

The production and dissipation of the turbulent kinetic energy also show the same trend, indicating that the overall turbulence activity is weakened by the control (figure 10). The locations of the maximum production are at $y^+ \approx 12$ for the unmanipulated channel and 17 for the manipulated channels, which also correspond to the locations of the maximum streamwise turbulence intensity.

Figure 11 shows the profile of root-mean-square pressure. The pressure fluctuations are substantially reduced throughout the channel with both control schemes. The reduction of the surface-pressure fluctuation is especially notable since this implies that one can also reduce the structure-generated noise within the turbulent boundary layer simultaneously with the skin friction.

4.3. *Reynolds shear stress and quadrant analysis*

The Reynolds shear stress, $-\overline{u'v'}$, is shown in figure 12. Also shown in figure 12 (*a*) is the total shear stress, $-\overline{u'v'} + (1/Re_{\tau_u})\partial\bar{u}/\partial y$, where $Re_{\tau_u} = u_{\tau_u}\delta/\nu$ and u_{τ_u} is the wall-shear velocity for the unmanipulated channel flow (table 1). In the fully developed channel flow considered here, this profile should be straight line when the flow reaches an equilibrium state. The computed results clearly indicate that this is the case. The slight oscillations are due to the small sample used to compute the statistics, i.e. only a single field is used to compute the total stress. The slope of the total shear stress is reduced by the control schemes. Also, there is a significant reduction in the Reynolds shear stress throughout the channel. There is a noticeable region around $y^+ \approx 5$ in which Reynolds shear stress is nearly zero.

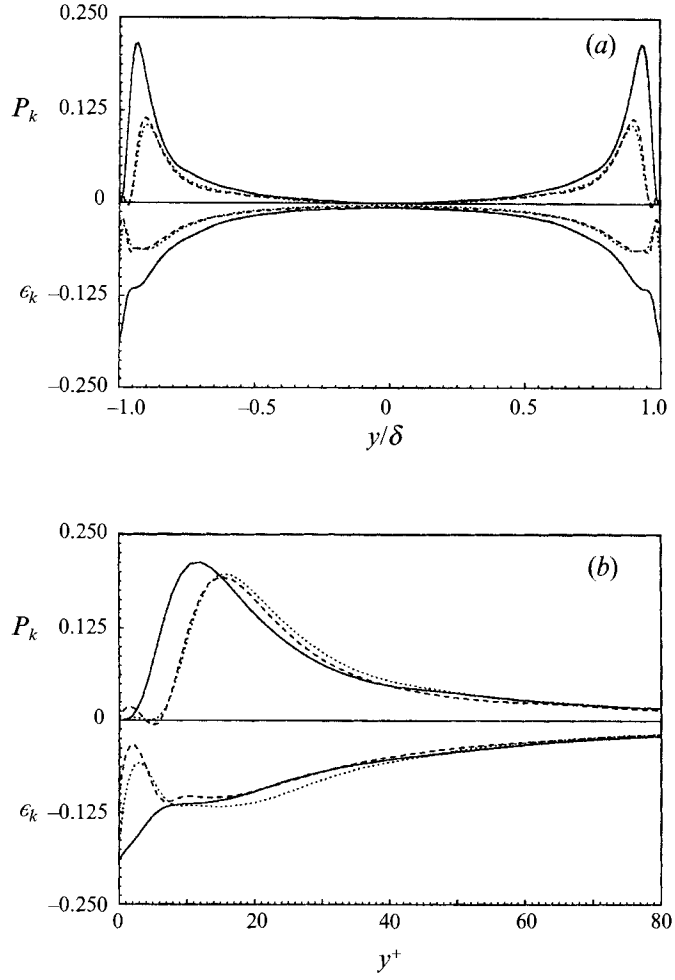

FIGURE 10. Production (P_k) and dissipation (ϵ_k) of the turbulence kinetic energy: —, no control; – – –, v-control; · · · · · · · · ·, w-control. (*a*) In global coordinates; (*b*) in wall coordinates. In wall coordinates, values are non-dimensionalized by the actual wall-shear velocity.

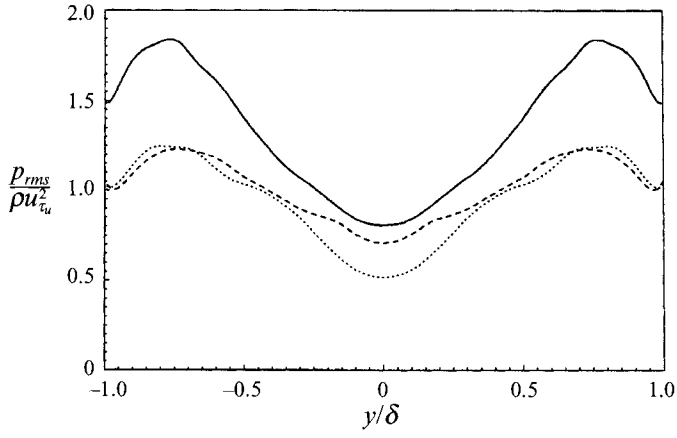

FIGURE 11. Root-mean-square pressure fluctuations normalized by the wall-shear velocity, u_{τ_u}: —, no control; – – –, v-control; · · · · · · · · ·, w-control.

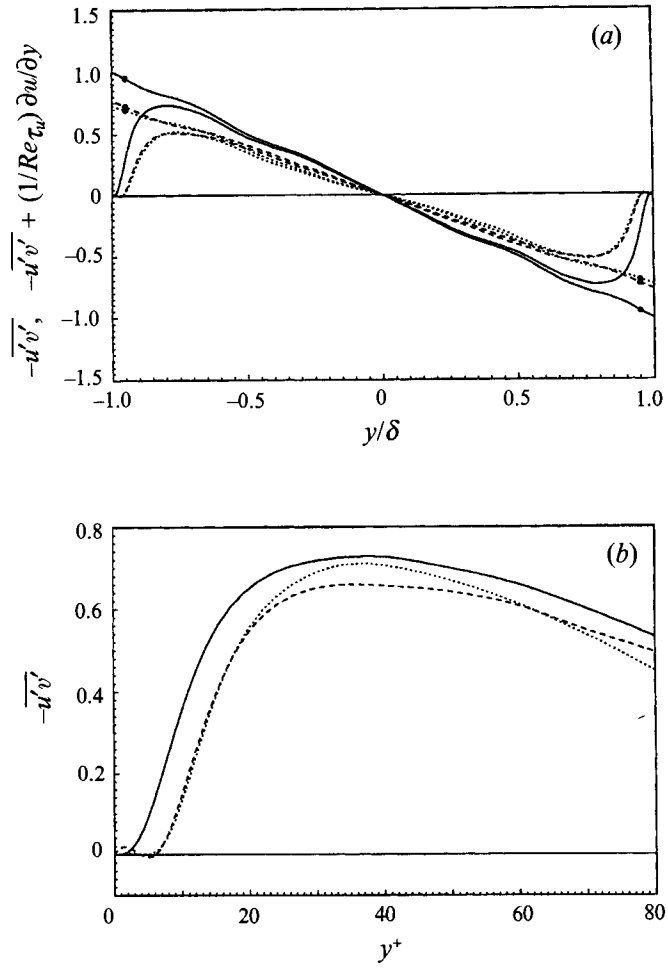

FIGURE 12. Reynolds shear stress ($-\overline{u'v'}$; lines) and total shear stress ($-\overline{u'v'} + (1/Re_{\tau_u})\,\partial\bar{u}/\partial y$; lines with ●) normalized by the wall-shear velocity: —, no control; – – –, v-control; · · · · · · · , w-control. (*a*) In global coordinates; (*b*) in wall coordinates. In wall coordinates, values are non-dimensionalized by the actual wall-shear velocity.

The quadrant analysis of the Reynolds shear stress provides detailed information on the contributions to the total turbulence production from various events occurring in the flow (Wallace, Eckelmann & Brodkey 1972; Willmarth & Lu 1972). The second-quadrant ($u' < 0$ and $v' > 0$; ejection) and fourth-quadrant ($u' > 0$ and $v' < 0$; sweep) events contribute to the positive Reynolds shear stress (positive production), and the first-quadrant ($u' > 0$ and $v' > 0$) and third-quadrant ($u' < 0$ and $v' < 0$) events contribute to the negative Reynolds shear stress (negative production).

The contribution to the Reynolds shear stress from each quadrant normalized by the wall-shear velocity u_{τ_u} is shown in figure 13. The sum of the values at each position y from the four quadrants in figures 13 is equal to the local mean Reynolds shear stress. In the case of the unmanipulated channel, the ejection event is dominant away from the wall, and the sweep event is dominant in the wall region; at $y^+ \approx 12$, these contributions are about the same. In the manipulated channels, the Reynolds shear stress from the sweep and ejection events is significantly reduced by both controls. This mitigation of the positive Reynolds-shear-stress events is also observed in drag-reduced

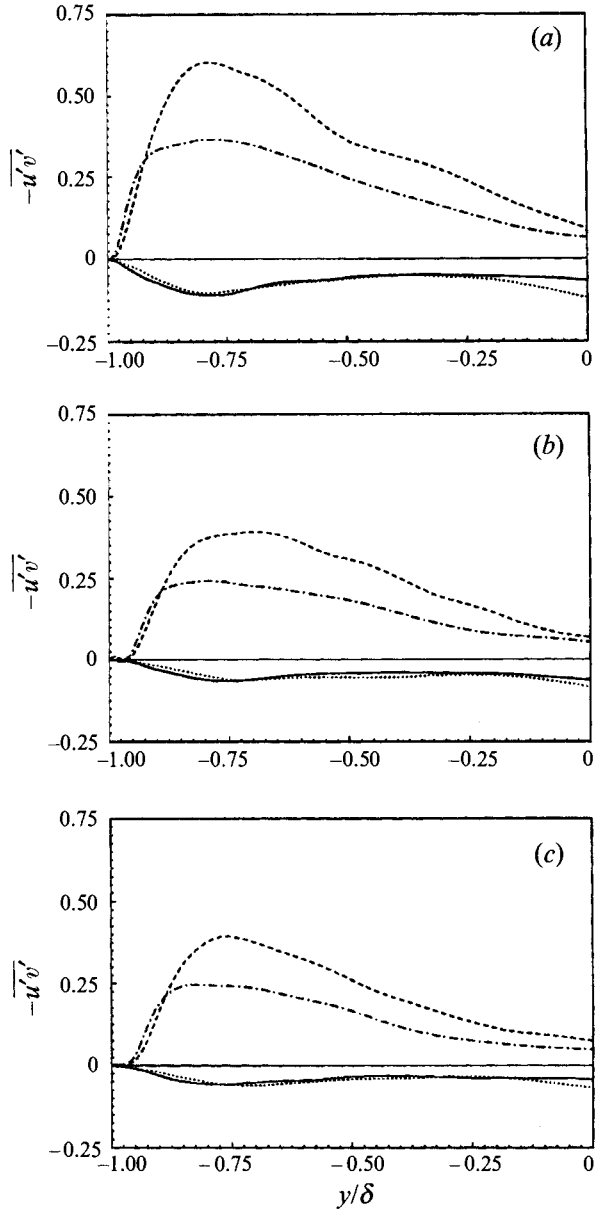

FIGURE 13. Reynolds shear stress from each quadrant normalized by the wall-shear velocity u_{τ_w}: —, first; – – –, second; · · · · · · · · ·, third; –·–, fourth quadrant. (*a*) No control, (*b*) *v*-control, (*c*) *w*-control.

flows over riblets (Choi *et al.* 1993). The fractional contribution from each quadrant event shows that there is no noticeable difference above $y^+ \approx 20$ except for an outward shift of the data; at $y^+ \approx 17$ the contributions from the ejection and sweep events are about the same (Choi, Moin & Kim 1992). That is, the active control schemes do not alter the structure of the outer-wall turbulence, but simply attenuate its strength and move the effective origin outward. The fourth-quadrant events are most dominant near the wall regardless of the control.

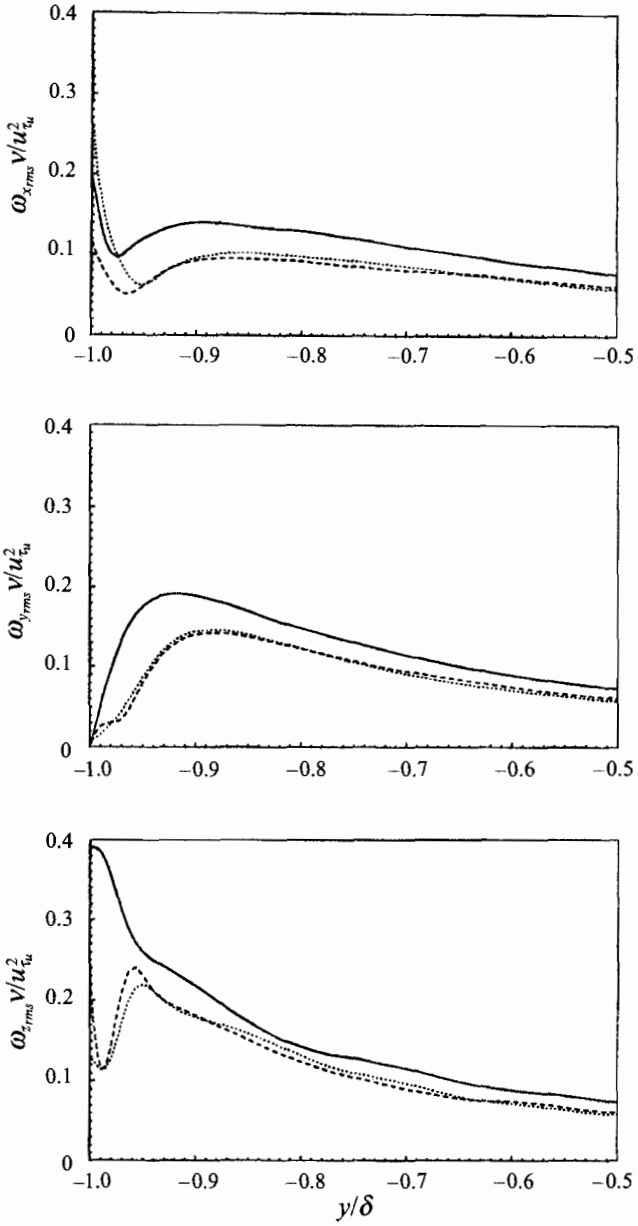

FIGURE 14. Root-mean square vorticity fluctuations normalized by the wall-shear velocity in global coordinates: —, no control; – – –, v-control; · · · · · · · · ·, w-control. Note that $y/\delta = -1$ corresponds to the lower location.

4.4. *Vorticity*

Root-mean-square vorticity fluctuations are shown in figure 14. All three components of vorticity fluctuations are substantially reduced throughout the channel with both control schemes. w-control increases the streamwise vorticity fluctuation at the wall while v-control reduces it as compared with the unmanipulated channel case. It is also interesting to note that the y-locations of the local maxima of the streamwise vorticity fluctuations in the manipulated flows are further away from the wall compared with that in the unmanipulated flow, suggesting that the sweep motion induced by the

streamwise vortices in the manipulated flows is less effective in producing a high-skin-friction region (Kravchenko, Choi & Moin 1993). The vorticity fluctuations in wall coordinates show that the major difference among the data sets is the apparent outward shift of the controlled data, as was discussed in §4.2.

Each component of the vorticity consists of two terms, i.e.

$$\omega_x = \frac{\partial w}{\partial y} - \frac{\partial v}{\partial z}, \quad \omega_y = \frac{\partial u}{\partial z} - \frac{\partial w}{\partial x}, \quad \omega_z = \frac{\partial v}{\partial x} - \frac{\partial u'}{\partial y}.$$

Regardless of the control scheme, near the wall, ω_x, ω_y and ω_z are mostly dominated by $\partial w/\partial y$, $\partial u/\partial z$ and $\partial u'/\partial y$, respectively (see Choi *et al.* 1992). The contributions of the normal velocity gradient to the magnitudes of the streamwise and spanwise vorticities are negligible near the wall.

Since the streamwise vorticity fluctuations are dominated by $\partial w/\partial y$, we experimented with a control scheme which altered the wall spanwise velocity in order to make $\omega_x = \partial w/\partial y = 0$ at the wall. This boundary condition is equivalent to using an in-phase control of the spanwise velocity, matching the spanwise velocity at the sensor location at the grid point nearest to the wall. A significant increase of the skin friction was obtained, and the vorticity fluctuations as well as the velocity fluctuations were increased substantially.

Despite the comparable drag reductions by both control schemes, w-control increases the streamwise vorticity fluctuation at the wall, while v-control reduces it as compared to the unmanipulated channel case (figure 14): the values of root-mean-square ω_x at the walls are 0.20 (no control), 0.12 (v-control) and 0.28 (w-control), respectively. Furthermore, the skin friction is significantly increased with the boundary condition $\omega_x|_w \approx 0$ (an in-phase w-control). It is well known that the existence of the streamwise vorticity at the wall in the unmanipulated boundary-layer flow is a kinematical result of the presence of the primary streamwise vortex above the wall and the no-slip boundary condition at the wall. In the case of v-control, the reduced magnitude of $\omega_{x_{rms}}$ at the wall simply represents the reduced strength of the streamwise vortex above the wall, considering that the control input velocity (blowing/suction) by itself does not change the value of the streamwise vorticity at the wall ($\partial v/\partial z|_w \ll \partial w/\partial y|_w$). However, in the case of w-control, the input velocity directly changes the value of the streamwise vorticity at the wall. The out-of-phase w-control which increases the streamwise vorticity fluctuation at the wall significantly retards the cross-flow motion induced by the streamwise vortices above the wall. On the other hand, the boundary condition $\omega_x|_w \approx 0$ enhances the cross-flow motion, resulting in drag increase.

It turns out that the streamwise vorticity of the wall plays an important role in the wall-layer dynamics. Once lifted by the primary vortex of opposite sign, the system of two vortices will have an induced motion away from the wall and being of opposite sign they tend to cancel each other. Both the motion away from the wall and the cancellation process contribute to lower induced skin friction. This dual role of the secondary streamwise voriticity at the wall is consistent with the results of our control experiments. For example, the observed drag increase in the calculations with $\omega_x|_w \approx 0$ boundary condition is consistent with the elimination of the stabilizing role of the streamwise vorticity at the wall. See §5 for further discussion of the role of the streamwise vorticity at the wall.

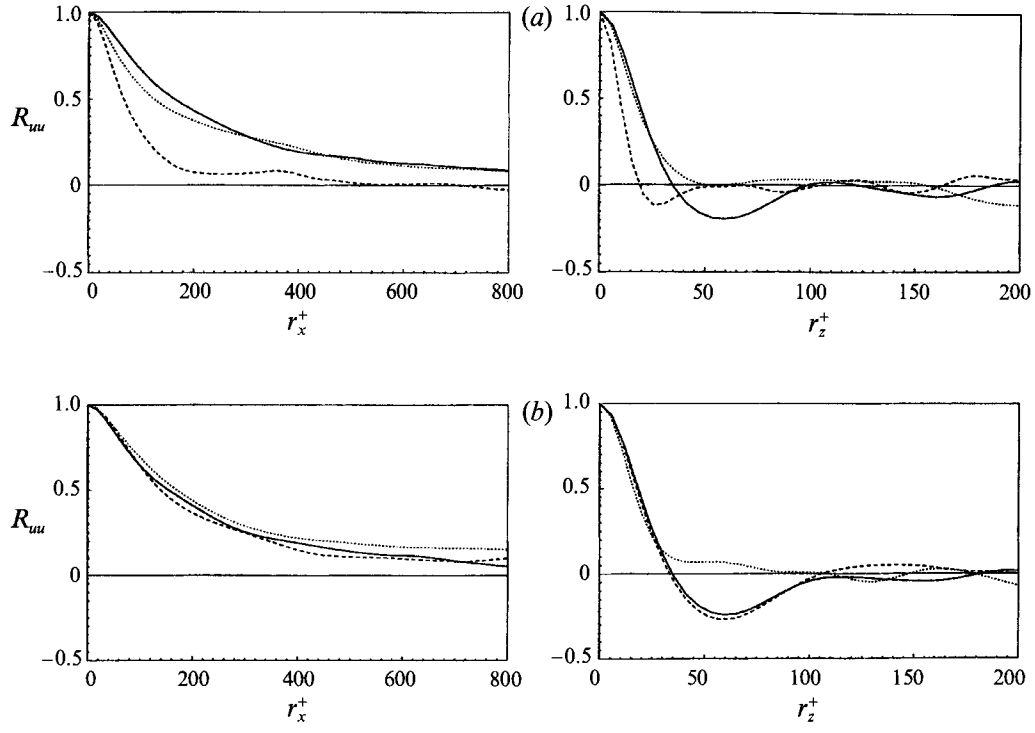

FIGURE 15. Two-point correlations of the streamwise velocity fluctuation: —, no control; – – –, v-control; · · · · · · · · ·, w-control. (*a*) At $y^+ \approx 0.2$; (*b*) at $y^+ \approx 10$.

4.5. *Two-point correlation functions*

Two-point velocity correlations are shown in figure 15 for both control cases, and are compared to those of the uncontrolled channel flow. The spanwise two-point correlations may indicate that the velocity fields are modified in different ways. In the unmanipulated channel, the locations of the local minima of spanwise two-point correlations of the streamwise and spanwise velocities are nearly identical ($r_z^+|_{min} \approx 50$) below $y^+ \approx 10$, while $r_z^+|_{min} \approx 25$ for the normal velocity component (Kim *et al.* 1987). In both controlled flows, below $y^+ \approx 5$, the streamwise microscale, which is defined by the curvature of the streamwise two-point correlation of u' at $r_x^+ = 0$, is significantly reduced, as compared to that in the uncontrolled flow, indicating that the streaky structures have disappeared in that region in the manipulated channels. In the case of v-control, the two-point correlation of the streamwise velocity at $y^+ \approx 0.2$ is similar to that of the normal velocity at that location (Choi *et al.* 1992); the structure of the streamwise velocity very near the wall is clearly affected by the action of blowing and suction. Near $y^+ \approx 10$, the qualitative behaviour of two-point correlation of u' in the v-controlled channel is similar to that in the unmanipulated channel. In the case of w-control, the streamwise two-point correlations of the velocities are similar to those in the unmanipulated channel except that the streamwise microscale at $y^+ \approx 0.2$ is reduced. However, the spanwise two-point correlations of the streamwise velocity do not clearly show a negative minimum near the wall region.

At low Reynolds numbers the mean streak spacing can be obtained from the two-point correlation of the streamwise velocity. The mean spacing between streaks is roughly twice the separation distance of the negative minimum of the spanwise correlation of the streamwise velocity. Owing to the lack of streaky structures very near

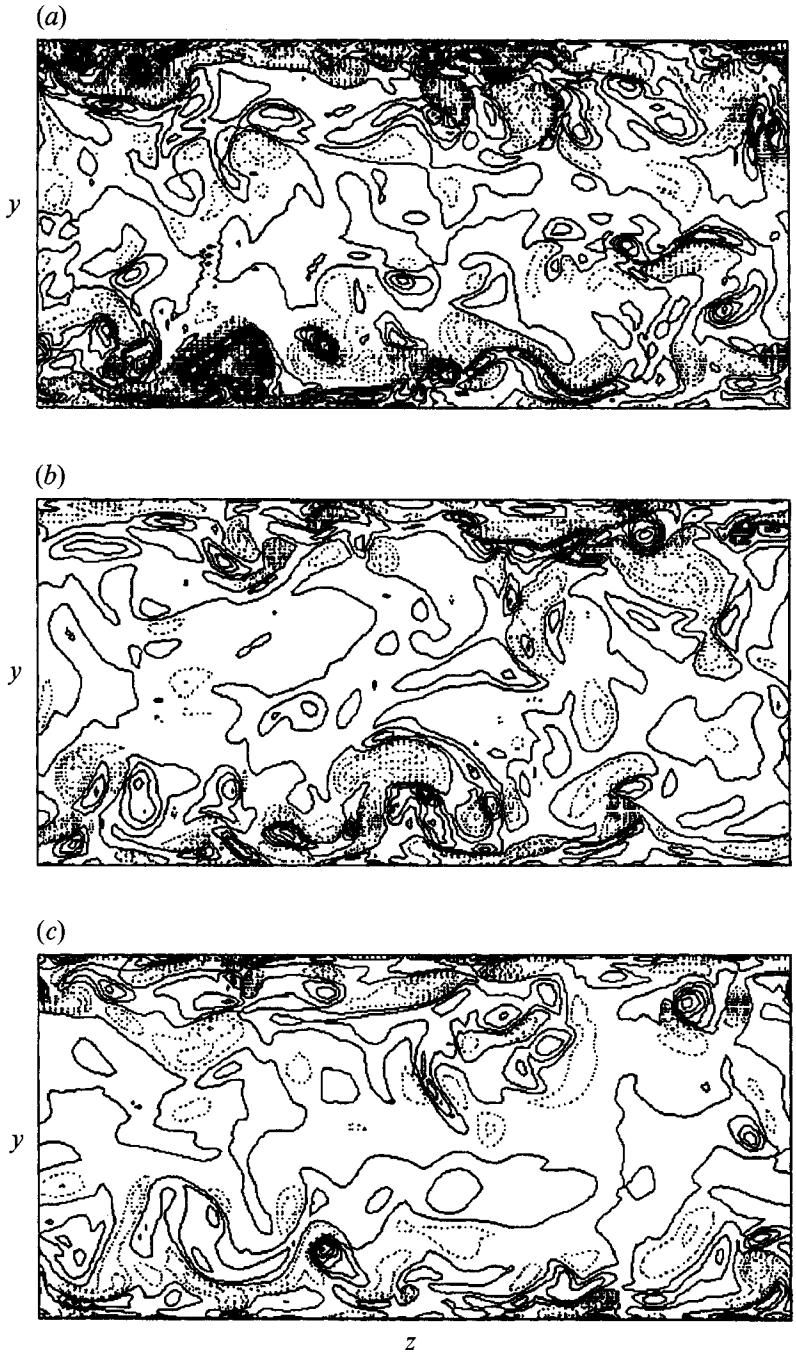

FIGURE 16. Contours of streamwise vorticity fluctuations in a cross-flow plane. The contour levels range from $\omega_x \delta / u_{\tau_u} = -120$ to 120 by increments of 10. Negative contours are dotted. The plot domain extends from the lower wall to the upper wall in y. (*a*) No control, (*b*) v-control, (*c*) w-control.

the wall ($y^+ < 5$) in the manipulated channels, streak spacings cannot be obtained for that region. For $5 < y^+ < 10$, the mean streak spacing is increased in the v-controlled channel, and it has nearly the same value above $y^+ \approx 10$ as in the unmanipulated channel (figure 15). In the w-controlled channel, however, the two-point correlation of

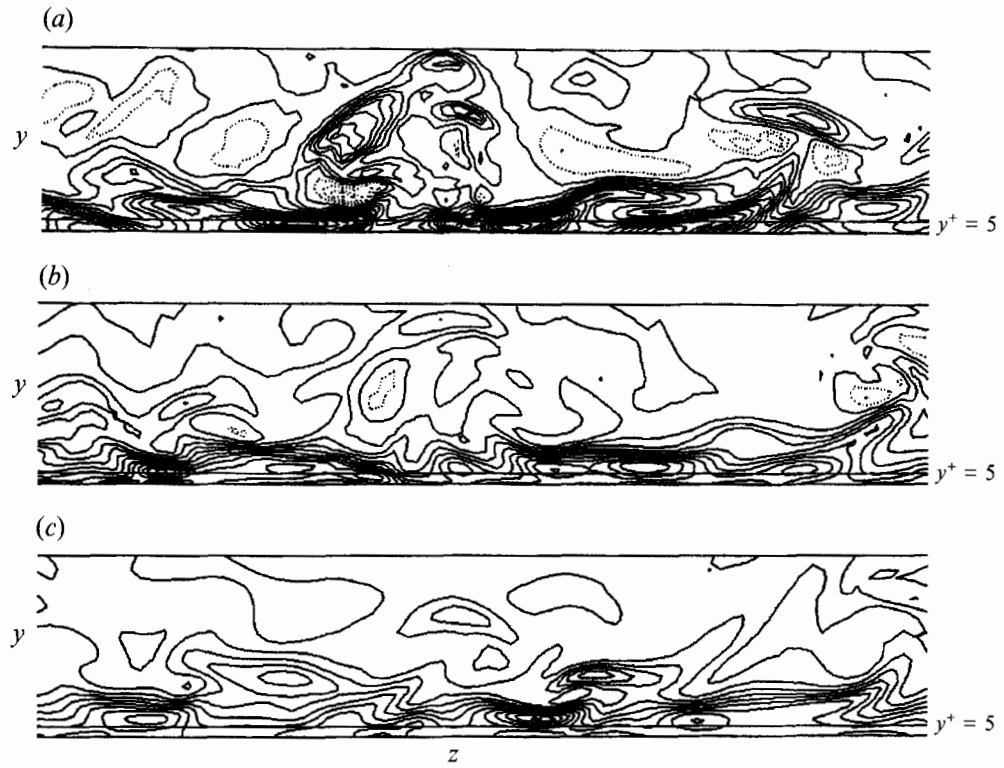

FIGURE 17. Contours of spanwise vorticity fluctuations in a cross-flow plane. The contour levels range from $\omega_z \delta / u_{\tau_u} = -340$ to 100 by increments of 20. Positive contours are dotted. The plot domain extends from $y/\delta = -1$ (lower wall) to $y/\delta = -0.5$. (*a*) No control, (*b*) *v*-control, (*c*) *w*-control.

the streamwise velocity does not clearly show a negative minimum up to $y^+ \approx 10$ even though streaky structures appear to exist in the instantaneous flow fields (see Choi *et al.* 1992), which suggests that there exists a broad range of spanwise dimensions of streaky structures in the *w*-controlled channel. Note that we have used the actual wall-shear velocity u_τ when the mean streak spacing (or the separation distance r_z^+) is calculated in wall units. Hence the physical dimension of the mean streak spacing in the manipulated channels is actually larger than that in the unmanipulated channel above $y^+ \approx 10$.

Two-point correlations of the wall-shear rate and wall pressure were also investigated (for more details, see Choi *et al.* 1992). The streamwise integral scale of the wall shear-rate fluctuation was significantly reduced by the controls. The two-point correlation of the wall pressure, however, was changed very little by the control schemes, indicating that the scales of the turbulence structures above the viscous sublayer, which strongly influence the wall-pressure fluctuations (Kim 1989), have not been affected by the control action.

5. Turbulence structure of the manipulated channel flows and drag-reduction mechanisms

As mentioned in §4, turbulence statistics in the manipulated channels are substantially different from those in the unmanipulated channel. A relatively small amount of either blowing and suction or spanwise velocity at the surface appreciably

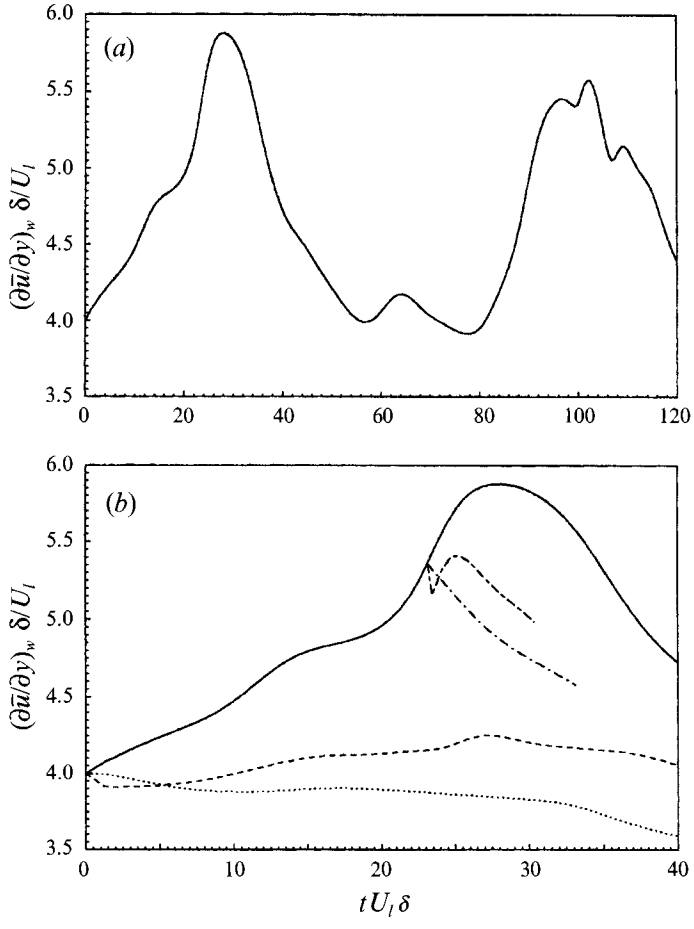

FIGURE 18. Time history of the horizontally averaged wall-shear rate at the lower wall for minimal channel flow: (*a*) —, no control; (*b*) —, no control; – – –, *v*-control (SEQ1); · · · · · · · · ·, *w*-control (SEQ1); – –, *v*-control (SEQ2); – · –, *w*-control (SEQ2). $(\partial\bar{u}/\partial y)_w\ \delta/U_l = 2$ corresponds to fully developed laminar channel flow.

changes turbulence statistics throughout the channel. Differences between turbulence statistics of the *v*- and *w*-controlled channels reveal that, despite comparable drag reductions, the structures may have been affected differently. Also, the control strategies presented in §3 are not capable of eliminating the essential features of turbulence structures, but they are able to weaken most structures substantially. In this section, we focus on turbulence structures in the manipulated channels by examining instantaneous flow fields and study drag-reduction mechanisms caused by the active controls.

5.1. *Structure of manipulated channel flows*

Contour plots of the streamwise velocity of both manipulated channel flows in the wall region were compared to those of the unmanipulated channel flow. The streaky structures have disappeared or have been substantially weakened below $y^+ \approx 5$ in the manipulated channels, and at $y^+ \approx 10$ the mean streak spacing appeared to be larger than in the unmanipulated channel. Also, the active control schemes significantly reduced the magnitude of the streamwise velocity in the wall region. In the case of *v*-

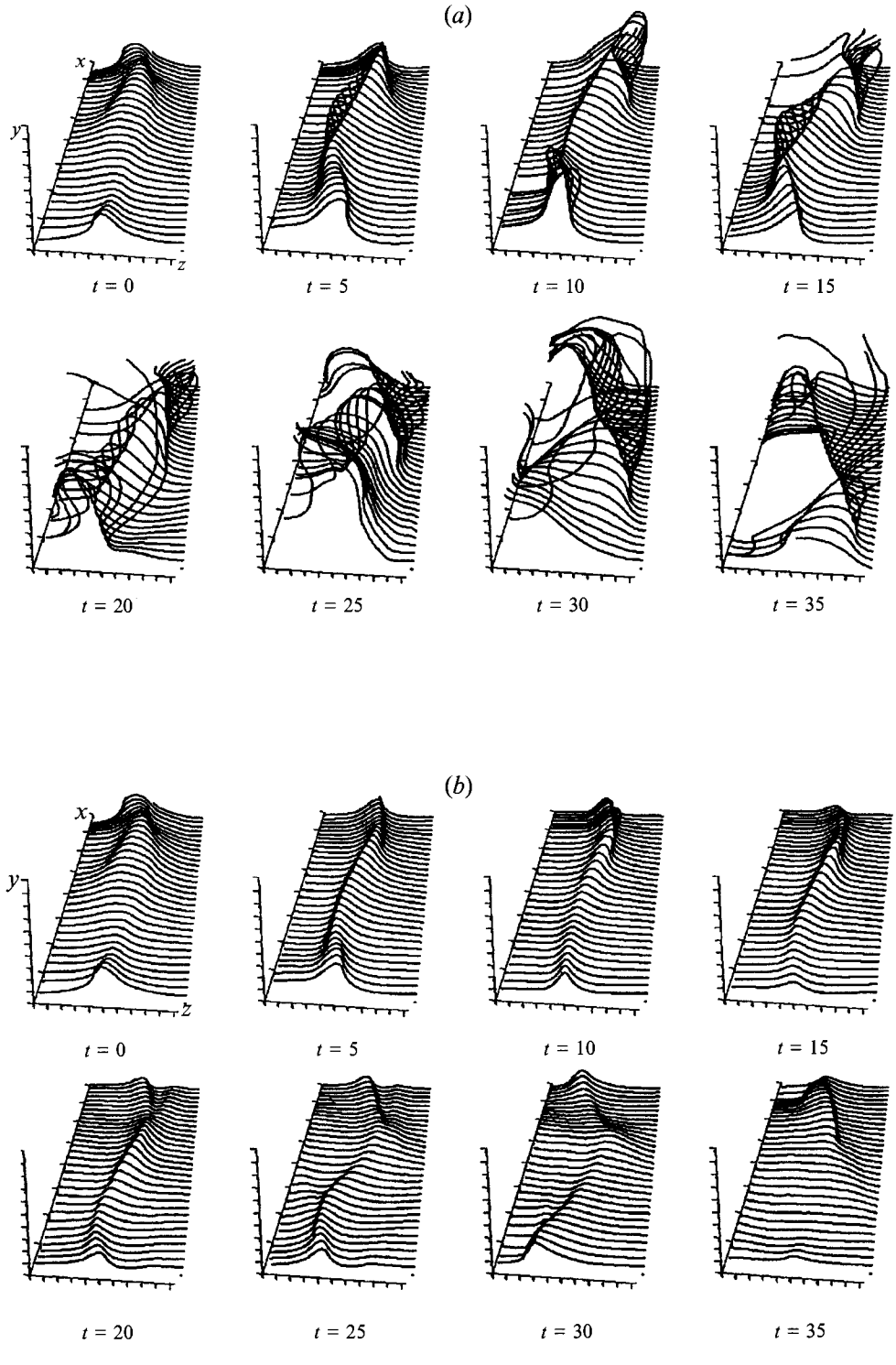

FIGURE 19(*a*, *b*). For caption see facing page.

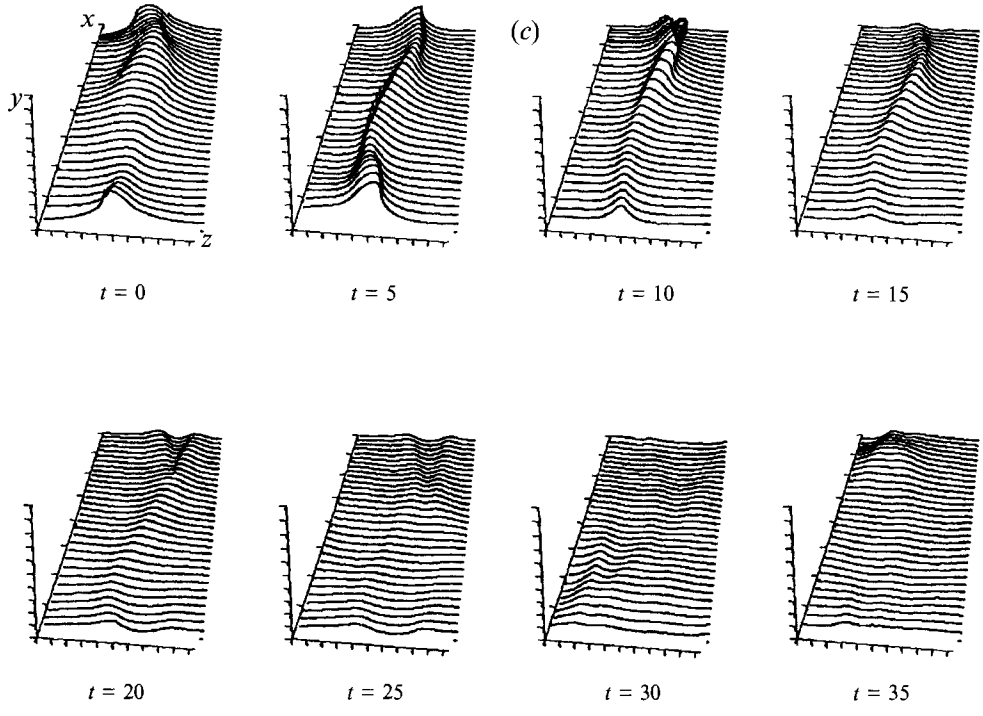

FIGURE 19. Time sequence of the evolution of the wall vorticity layer for minimal channel flow: (*a*) no control; (*b*) *v*-control; (*c*) *w*-control. Flow is along the *x*-direction. Vortex surface is initiated from the right edge of the computational domain at $y^+ \approx 7.5$. Full computational box ($L_x = \pi\delta$ and $L_z = 0.35\pi\delta$) is shown.

control, the contours of the streamwise velocity near the wall were similar to those of the wall-normal velocity. This observation was confirmed statistically with two-point correlations in §4.5.

Contours of instantaneous streamwise vorticity in a (y, z)-plane in the manipulated and unmanipulated channels are shown in figure 16. The reduction in the intensity of the streamwise vorticity near the wall is apparent. Figure 17 shows the contours of instantaneous spanwise vorticity in a (y, z)-plane. The intensity is, again, significantly reduced. The high-shear-rate regions near the unmanipulated wall do not appear near the manipulated walls. Instead, these high-shear-rate regions are shifted slightly to the interior ($y^+ \approx 5$) of the manipulated channel by the action of the controls. This is one important drag-reduction mechanism and will be described in detail in the following section.

5.2. *Drag-reduction mechanisms of active controls*

In this subsection, we focus on the dynamics and underlying mechanisms that lead to the reduction in drag and the strength of the large-scale structures. We employ two approaches as outlined below.

In general, it is rather difficult to study the dynamics associated with a turbulent flow. The main reasons for this difficulty are twofold. First, at any given instant, the flow is crowded with several structures at a broad range of scales and the associated complex interactions. Second, it is difficult to follow the temporal evolution of a given structure over a long period of time. The approach in the present study is based on the work of Jiménez & Moin (1991), which demonstrated that the essential dynamics

associated with the streamwise vortical structures present in the wall region can be reproduced in what they referred to as the 'minimal channel' flow. In their study, the computational box size in the streamwise and spanwise directions was sufficiently small such that it could only accommodate one or two vortical structures while maintaining turbulence. It is a relatively easy task then to follow the evolution of a single vortical structure in this manner. Of course, some interactions between different structures are absent in the minimal channel flow. However, since the near-wall turbulence statistics were reproduced accurately, Jiménez & Moin implied that such interactions may not be essential to turbulence dynamics in the wall region. Computed flow fields in the minimal channel with both v- and w-control strategies implemented are analysed below to investigate the dynamics associated with a streamwise vortex.

In the second approach, we examine an even simpler model problem. To gain further insight into how the surface boundary condition interacts with a streamwise vortex, we performed numerical simulations of an isolated vortex dipole interacting with a wall, with and without control manipulations.

5.2.1. *Minimal channel flow*

The database of Jiménez & Moin (1991) is used as the base flow for control. The Reynolds number based on the corresponding laminar centreline velocity U_l and channel half-width δ is 2000. The computational box for this particular Reynolds number is $\pi\delta$, 2δ and 0.35δ in the x-, y- and z-directions, respectively. At this particular Reynolds number, the flow is turbulent at only one wall. Jiménez & Moin (1991) chose this Reynolds number in order to study the structure of the vorticity field because flow features are 'cleaner' at low Reynolds numbers, but similar features are also observed at higher Reynolds numbers where both walls are turbulent.

Figure 18(*a*) shows the time history of the horizontally averaged wall-shear rate in the unmanipulated channel from $tU_l/\delta = 0$ to 120. In this period, there are two *intermittency* cycles according to Jiménez & Moin (1991). In each cycle, all turbulence intensities as well as the wall-shear rate vary strongly. The velocity fields at $tU_l/\delta = 0$ and 23.1 were used as initial flows to apply both control schemes. The latter flow field was chosen during the turbulence activation period. SEQ1 denotes the evolution of the flow fields with the initial flow of $tU_l/\delta = 0$ and SEQ2 the evolution of the flow fields with the initial flow of $tU_l/\delta = 23.1$. The modified wall-shear rates due to the controls are shown in figure 18 (*b*). The wall-shear rates are significantly reduced in both SEQ1 and SEQ2. Intensities of the velocity and vorticity fluctuations are also considerably reduced. The controlled flow fields (SEQ1 and SEQ2) were stored in time increments of $tU_l/\delta = 5$ ($tu_\tau^2/\nu \approx 24$) and visually analysed and compared to the corresponding unmanipulated sequences.

Regions of high skin friction are closely related to the location and strength of streamwise vortices near the wall (Kim *et al.* 1987; Kravchenko *et al.* 1993). The sweep motion due to strong streamwise vortices creates high-skin-friction regions on the wall. Most of the vorticity in the wall region is spanwise owing to the mean shear. Further from the wall where streamwise vortices are located ($y^+ = 15$–40) this is no longer true, and the three vorticity components have comparable magnitudes. Possible origins of the strong streamwise vortices are the tiling of the ω_z-dominated vortex lines by spanwise variation of the streamwise velocity ($\omega_z \partial u/\partial z$) and tilting of the normal vorticity by the prevailing shear ($\omega_y \partial u/\partial y$).

Time sequences of the evolution of the wall-vorticity layer in the manipulated and unmanipulated channels (SEQ1) are shown in figure 19. Each frame in the time sequence shows an instantaneous view of the position of the sheet as it approaches the

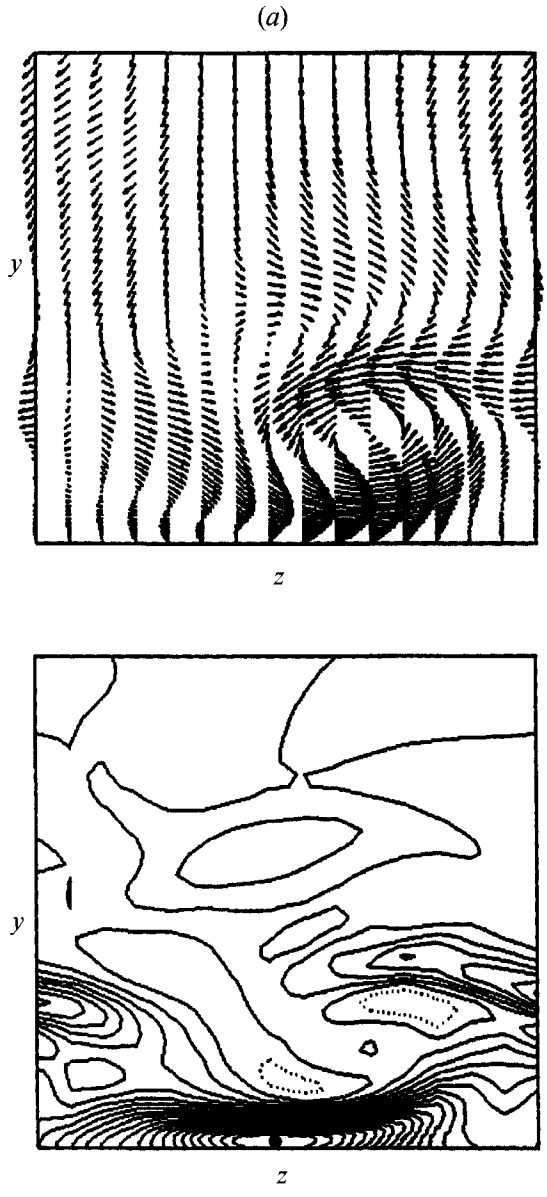

FIGURE 20(*a*). For caption see p. 103.

active peak in the intermittency cycle shown in figure 18. The surface is marked by individual transverse vortex traces initiated at $y^+ \approx 7.5$ in a relatively undisturbed part of the layer. In the unmanipulated channel, the lifting of the layer away from the wall over the low-velocity streak is evident, as is the waviness of the streak itself. The lifting process is mainly due to a strong streamwise vortex above the wall (Jiménez & Moin 1991). A short time after applying control, the lifting of the vortex layer essentially disappears. The vortex lines modified by the active control schemes are mainly composed of the spanwise vorticity near the wall, and the absence of tilting and lifting of the spanwise vorticity prevents new formation of the streamwise vorticity above the wall. Vortex traces initiated at $y^+ \approx 5$ and 10 followed the same trend. It is interesting

(*b*)

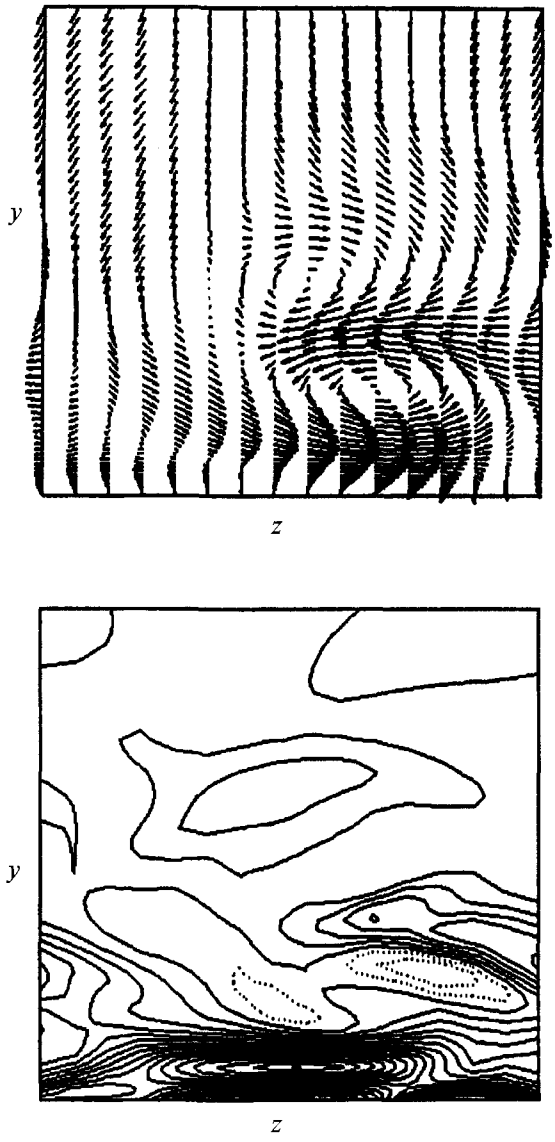

FIGURE 20(*b*). For caption see facing page.

to note that both controls eventually result in laminar flow solutions. Since laminarization did not occur in the full channel simulations. at nearly the same Reynolds number (§§3.1 and 3.2), it is probably a consequence of the use of the minimal flow unit.

The time history of the skin fraction on the manipulated walls shows that the skin friction decreases as soon as the control is applied to the flow even though the primary streamwise vortex above the wall is not immediately affected. Therefore, there must be another drag-reduction mechanism besides the reduction of the strength of the streamwise vortex above the wall. In order to investigate this effect more clearly, we applied both controls at $tU_l/\delta = 23.1$, when the skin friction is increasing very rapidly

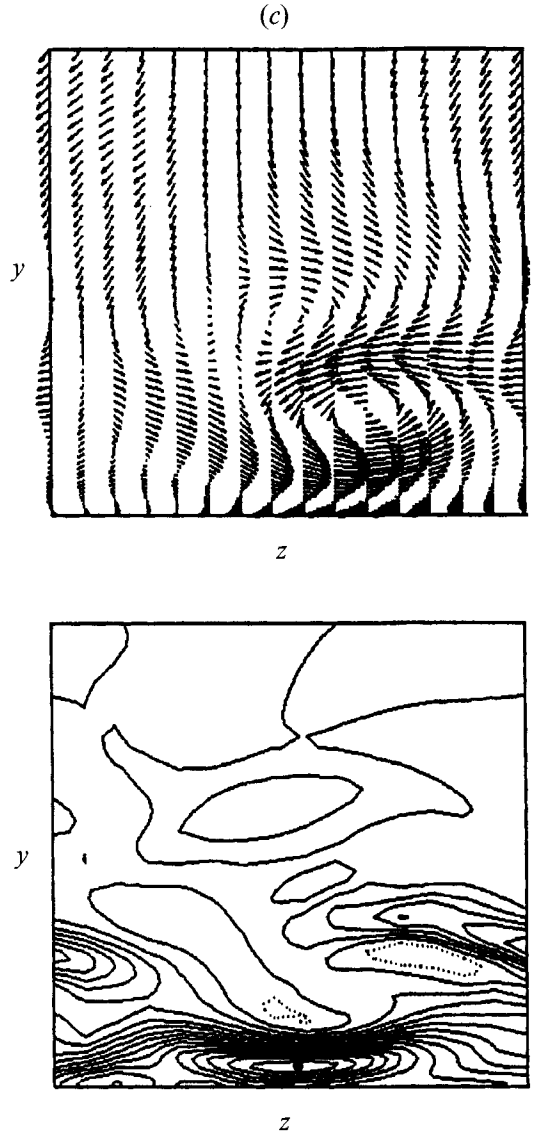

FIGURE 20. Velocity vectors (v, w) and contours of the spanwise vorticity in a (y, z)-plane: (*a*) no control; (*b*) v-control; (*c*) w-control. The contour levels range from $\omega_z \delta / U_l = -10$ to 2 by increments of 0.5. Positive contours are dotted; ● denotes the location of the maximum spanwise vorticity. The plot domain extends from the lower wall to the centreline.

on the unmanipulated wall (figure 18). An abrupt decrease of the wall-shear rate was found with both control schemes. Figure 20 shows cross-flow velocity vectors (v, w) and contours of the spanwise vorticity in a (y, z)-plane at $tU_l/\delta = 30$, when there is a significant reduction of the skin friction in the manipulated cases (SEQ2). The figure shows that turbulence structures remain essentially unchanged except very near the wall. The high-shear-rate regions on the wall are moved to the interior of the channel ($y^+ \approx 5$) by the control schemes. The sweep motion due to strong vortices is directly deterred by active controls. A schematic diagram of the drag-reduction mechanism is shown in figure 21. Note that, in the case of w-control, a wall-normal velocity is

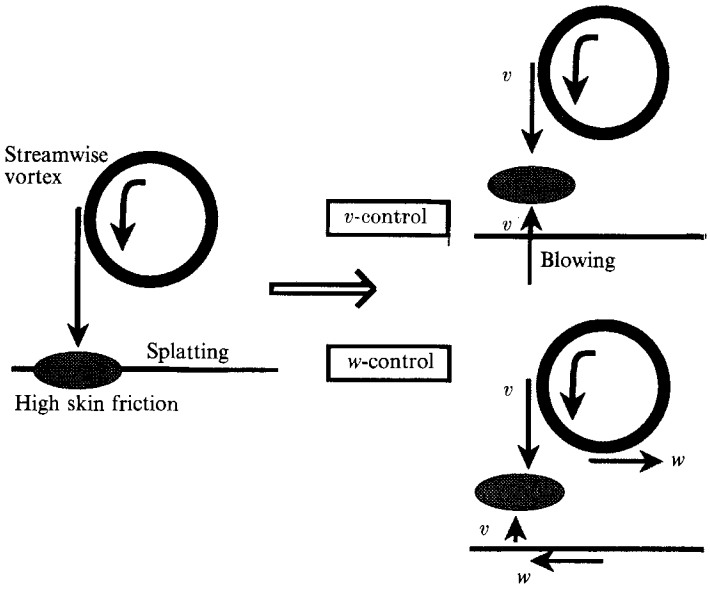

FIGURE 21. Schematic diagram of a drag-reduction mechanism by active controls in a cross-flow plane.

induced very near the wall by the imposed spanwise velocity distribution at the wall; from the continuity equation at the wall, $\partial v/\partial y = -\partial w/\partial z \neq 0$, leading to higher values of v near the wall.

5.2.2. *An isolated vortex interacting with a wall*

Although the minimal flow unit is a useful tool for tracing turbulence structures in time, the flow in the minimal channel is still too complicated to easily isolate the effect of the control schemes on the primary streamwise vortices above the wall. To gain further insight into how the control affects the dynamics of the streamwise vortices, a two-dimensional vortex pair interacting with a wall with and without boundary manipulation was simulated. Of course, the results described below represent a highly idealized situation, because there are no mechanisms for stretching or tilting of vortices in this flow. The strength of the primary vortex pair in this simulation continuously decreases owing to viscous diffusion.

The Reynolds number of the initial vortex dipole is $Re_\Gamma = \Gamma/\nu = 1800$, where Γ is the circulation of the vortex, and ν is the kinematic viscosity. The strength of this vortex is much larger than those observed in turbulent boundary-layer flows; it was chosen to highlight the control effects more clearly. The size of the computational box is chosen to be $2\pi\delta$ and 2δ in the z- and y-directions, respectively, where δ is the channel half-width. The computations are performed using 128×65 spectral modes (spanwise and normal to the wall). The vortex dipole is initially located at the centre of the channel. Owing to the self-induced motion of the vortex dipole, it approaches the lower channel wall ($y = -\delta$). The sensor location for control was chosen to be at $y = -0.83\delta$. Two other sensor locations ($y = -0.94\delta$ and -0.67δ) gave similar results.

Figure 22 shows the time sequences of the vorticity in the manipulated and unmanipulated channels. In the unmanipulated channel, the vortex behaviour is similar to Orlandi's (1990) results. A vortex near a no-slip wall induces secondary

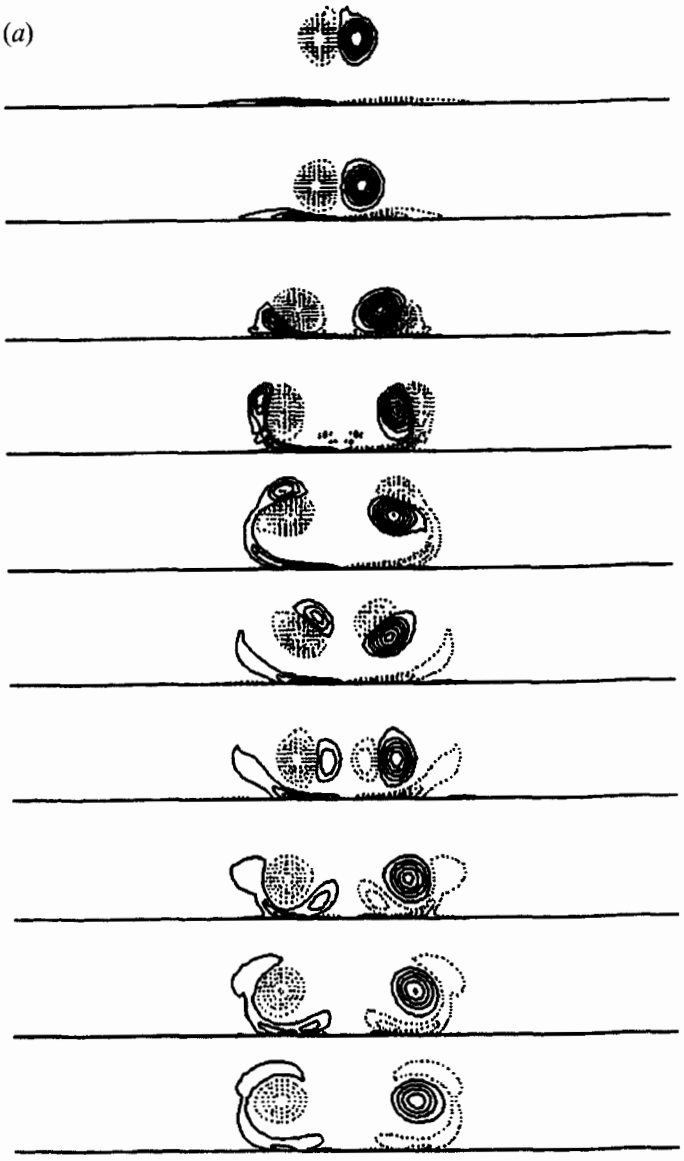

FIGURE 22(*a*). For caption see p. 107.

vorticity of opposite sign at the wall and carries it away to generate a new free vortex (figure 22*a*). The lifted secondary vortices inhibit the separation of the primary vortices. In the v-control scheme shown in figure 22 (*b*), the vortices separate. Here, the lifting of the secondary vorticity at the wall is clearly eliminated, and the y-location of the centre of the primary vortices stays nearly constant owing to the absence of the lifted secondary vorices. Thus, in the v-controlled flow, the control scheme changes the interaction between the primary vortex and the secondary vorticity by preventing the lifting process.

On the other hand, the vortex motion in the w-controlled channel lifting of the secondary vorticity. However, the difference is that stronger secondary vortices are created at the wall by the w-control scheme. Hence, the primary vortices are lifted further into the interior of the channel by the lifted stronger secondary vortices

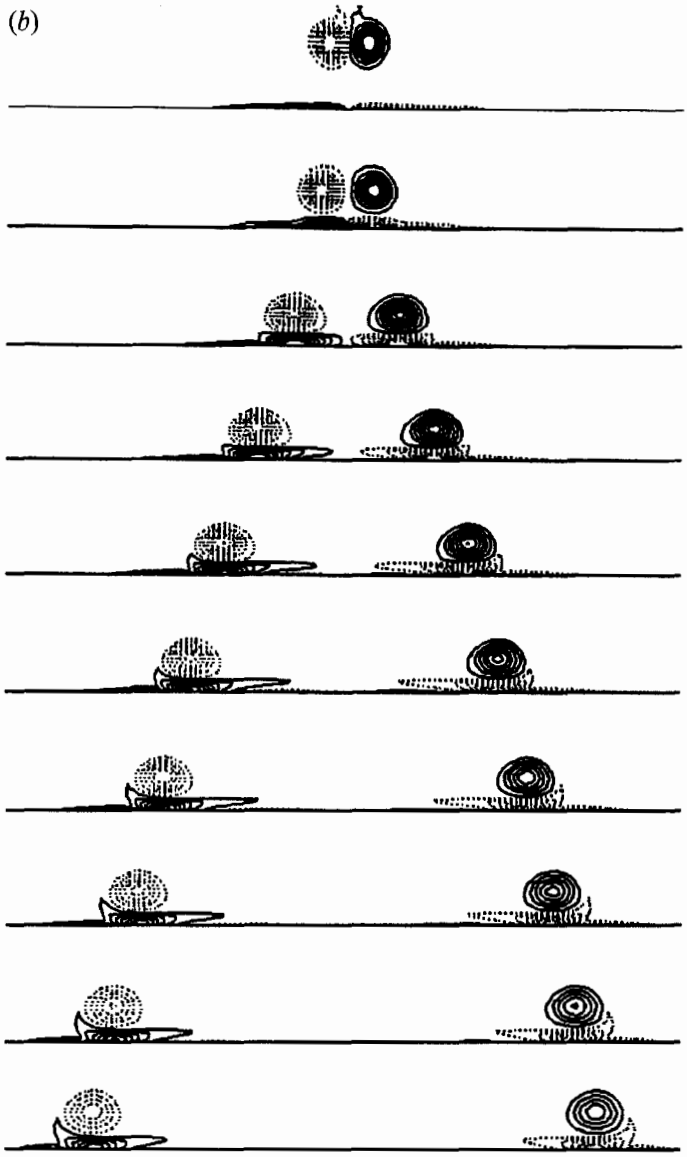

FIGURE 22(*b*). For caption see facing page.

(compare the y-locations of the centres of the primary vortices at their highest elevations in figures 22*a* and *c*), so that the sweep effect near the wall is reduced. The vortex rebounding time (Orlandi 1990) is also increased by the stronger secondary vortices.

The maximum value of the vorticity and the circulation of the primary vortices are not significantly changed by the control actions, indicating that the active control schemes applied do not directly reduce the strength of the primary vortices, but change their relative locations and interactions with the wall.

In order to investigate the effect of the streamwise vortex dipole on the mean skin friction on the wall, we performed numerical simulations in which a parabolic streamwise velocity was superimposed on the streamwise vortex dipole. Skin-friction reduction was found using both control schemes as compared to the uncontrolled case.

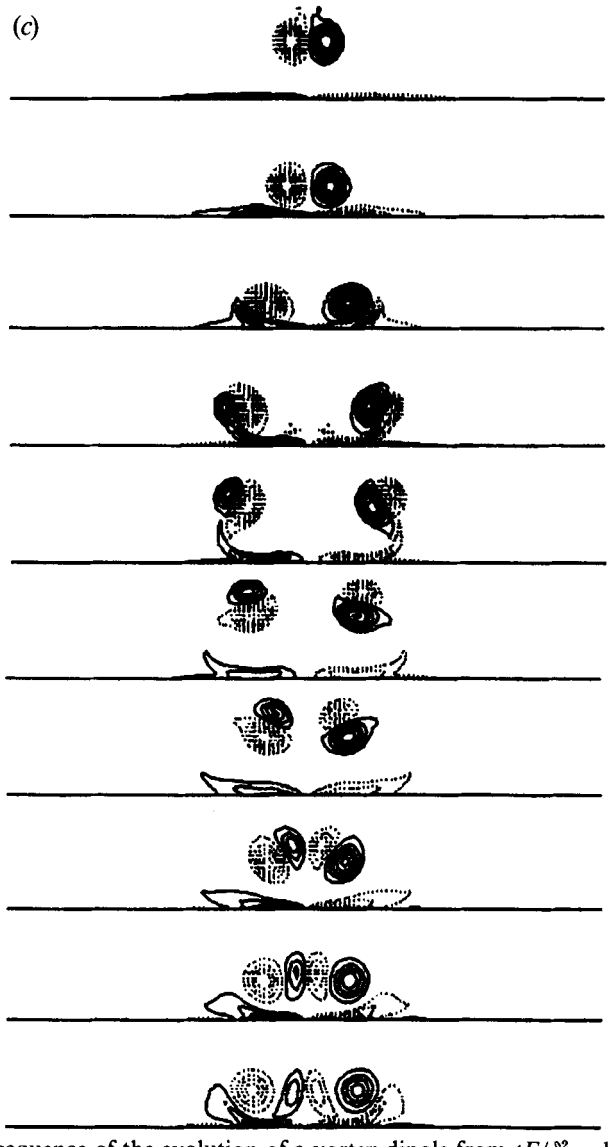

FIGURE 22. Time sequence of the evolution of a vortex dipole from $t\Gamma/\delta^2 = 1$ to 10 with increments of 1: (*a*) no control; (*b*) *v*-control; (*c*) *w*-control. The flow fields from $t\Gamma/\delta^2 = 0$ to 1 are identical regardless of boundary manipulations. Time increases from top to bottom. The contour levels of the vorticity ($\omega_x\delta^2/\Gamma$) range from -15 to 15 by increments of 2. Negative contours are dotted.

6. Summary and discussion

Active control strategies were investigated for the purpose of drag reduction using direct numerical simulation of turbulent channel flow. These included controls with the normal, spanwise and streamwise velocities, control with selective normal velocity, and control with the sensors at the wall. The skin-friction reduction was measured in terms of the change in the mean pressure gradient necessary to drive the flow with a fixed mass flow rate. The algorithm was based on the input velocity at the wall being proportional to the instantaneous velocity at a location near the wall. For instance, in the case of the normal-velocity control, the blowing or suction velocity at the wall was exactly opposite to the normal component of the velocity at a prescribed y-location, y_d.

The optimum location for matching the velocity was $y_d^+ \approx 10$. Approximately 20–30% reduction in the skin friction was achieved by controlling either the normal or the spanwise velocity at the wall.

In selective control experiments which affected only the strong events, the input control velocity was applied at the surface only when the normal velocity at the sensor location y_d exceeded a threshold value, v_{th}. In comparison to the 25% reduction for $v_{th} = 0$, 20% and 15% reductions were obtained with $v_{th} = v_{rms}$ and $v_{th} = 2v_{rms}$, respectively, where v_{rms} is the root-mean-square value of the normal velocity at $y = y_d$. Only 25% and 5%, respectively, of the total surface area were controlled, indicating that most of the drag reduction was indeed due to the suppression of the stronger events.

Control of turbulent boundary layers by placing sensors only at the wall was investigated for practical implementation. It was found that $g_w = \partial/\partial z\ (\partial w/\partial y)|_w$, which is a leading term in the Taylor series expansion of v near the wall, was the best surface detection criterion for the vertical velocity away from the wall. A control based on this variable yielded about 6% drag reduction.

The present study was conducted at low Reynolds numbers and one may wonder whether the same results can be obtained at higher Reynolds numbers. Ultimately the answer to this question must be deduced from experiments or computations at higher Reynolds numbers than in this study. However, we believe that the present results will probably hold at higher Reynolds numbers because our control strategies were limited to the near-wall region and used inner-layer scaling. Supporting evidence for this assertion is provided by the performance of longitudinal riblets in reducing drag in turbulent boundary layer where comparable drag reductions have been reported at low (Choi *et al.* 1993) and high Reynolds numbers (Walsh 1982) with riblets of consistent dimensions in wall units. Note that control devices acting on the outer layer of turbulent boundary layer such as LEBUs (Guezennec & Nagib 1985) may not provide a consistent local drag reduction at different Reynolds numbers.

The statistics of the manipulated channel flows were compared to those of the unmanipulated channel flow. The mean velocity as well as turbulent intensities were altered by the boundary modification. An upward shift in the log law and an increase of the viscous-sublayer thickness were obtained in the manipulated channels, which had been observed previously in other drag-reduced flows. The major difference among the data sets was the apparent outward shift of the controlled data, suggesting a displaced virtual origin of the boundary layer and a thickened sublayer. The value of the outward shift of flow variables was approximately 5 wall units, which coincided with the increased viscous-sublayer thickness.

Velocity, pressure, and vorticity fluctuations as well as the Reynolds shear stress were significantly reduced throughout the channel. This change of turbulence intensity with the active control schemes was in sharp contrast to the result of using a compliant surface or longitudinal riblets, in which only modifications in the near-wall region were observed. Instantaneous flow fields showed that streaky structures below $y^+ \approx 5$ were clearly diminished by the active control, and the physical spacing of the streaky structure above $y^+ \approx 5$ was increased in the manipulated channels.

The active blowing and suction used in this study significantly affected turbulence statistics above the wall. On the other hand, studies of the effects of unsteady blowing and suction (e.g. Narasimha 1983) or passive control devices in the past had indicated only marginal effects on turbulence statistics in the interior of the flow. The difference appears to be due to the use of a feedback loop in this work, while the latter approaches are mostly passive to the changes in flow structures. Therefore, even in cases where the

mass input at the wall is applied *passively* at the 'bursting' frequency, useful interaction may not take place between control inputs and flow structure because of the randomness of turbulence structure in space and time (Bushnell & McGinley 1989).

Drag-reduction mechanisms were studied with two different approaches: a minimal channel flow and an isolated vortex pair interacting with a wall. Time sequences of the flow fields in the minimal channel showed that there were two essential drag-reduction mechanisms. Firstly, within a short time after control is applied, drag is reduced mainly by deterring the sweep motion without modifying the primary streamwise vortices above the wall. Consequently, the high-shear-rate regions on the wall are moved to the interior of the channel ($y^+ \approx 5$). Secondly, the active control changed the evolution of the wall vorticity layer by stabilizing and preventing lifting of the spanwise vorticity near the wall. The absence of this lifting process weakens a source of new streamwise vortices above the wall.

In order to isolate the effect of the control schemes on the dynamics of a primary streamwise vortex above the wall, a two-dimensional vortex dipole interacting with a wall was simulated with and without boundary manipulation. The effects of the normal and spanwise velocities at the wall on the primary streamwise vortex pair were significantly different. The v-control altered the mutual interaction between the primary vortex pair and the secondary vorticity by preventing the lifting of the secondary vorticity. On the other hand, the vortex motion with the spanwise-velocity control was quite similar to that in the unmanipulated channel. However, the stronger secondary vorticity created by the spanwise-velocity control changed the location of the primary vortex pair as well as the flow timescale.

This work was sponsored by the Air Force Office of Scientific Research under Contact No. F49620-93-1-0078 with Dr James McMichael as the technical monitor. We are also grateful for useful discussions with Professor William C. Reynolds and Mr Tom Bewley.

REFERENCES

ALFREDSSON, P. H., JOHANSSON, A. V. & KIM, J. 1988 Turbulence production near walls: the role of flow structures with spanwise asymmetry. In *Studying Turbulence Using Numerical Simulation Databases, Proceedings of the 1988 Summer Program of the Center for Turbulence Research, NASA-Ames and Stanford University*, pp. 131–141.

BANDYOPADHYAY, P. R. 1986 Review – mean low in turbulent boundary layers disturbed to alter skin friction. *Trans. ASME* I: *J. Fluids Engng* **108**, 127.

BUSHNELL, D. M. & MCGINLEY, C. B. 1989 Turbulence control in wall flows. *Ann. Rev. Fluid Mech.* **21**, 1.

CANTWELL, B. J. 1981 Organized motion in turbulent flow. *Ann. Rev. Fluid Mech.* **13**, 457.

CHOI, H., MOIN, P. & KIM, J. 1992 Turbulent drag reduction: studies of feedback control and flow over riblets. *Rep.* TF–55. Department of Mechanical Engineering, Stanford University.

CHOI, H., MOIN, P. & KIM, J. 1993 Direct numerical simulation of turbulent flow over riblets. *J. Fluid Mech.* **255**, 503.

CHOI, K.-S. 1989 Near-wall structure of a turbulent boundary layer with riblets. *J. Fluid Mech.* **208**, 417.

CORINO, E. R. & BRODKEY, R. S. 1969 A visual investigation of the wall region in turbulent flow. *J. Fluid Mech.* **37**, 1.

GUEZENNEC, Y. G. & NAGIB, H. M. 1985 Documentation of mechanisms leading to net drag reduction in manipulated turbulent boundary layers. *AIAA Paper* 85–0519.

HO, C. M. & HUANG, L. S. 1982 Subharmonics and vortex merging in mixing layers. *J. Fluid Mech.* **119**, 443.

HOOSHMAND, A., YOUNGS, R. A., WALLACE, J. M. & BALINT, J.-L. 1983 An experimental study of changes in the structure of a turbulent boundary layer due to surface geometry changes *AIAA Paper* 83–0230.

JIMÉNEZ, J. 1987 Bifurcations and bursting in two-dimensional Poiseuille flow. *Phys. Fluids* **30**, 3644.

JIMÉNEZ, J. & MOIN, P. 1991 The minimal flow unit in near-wall turbulence. *J. Fluid Mech.* **225**, 213.

JIMÉNEZ, J., MOIN, P., MOSER, R. & KEEFE, L. 1988 Ejection mechanisms in the sublayer of a turbulent channel. *Phys. Fluids* **31**, 1311.

JOHANSSON, A. V., ALFREDSSON, P. H. & KIM, J. 1987 Shear layer structures in near-wall turbulence. In *Studying Turbulence Using Numerical Simulation Databases, Proceedings of the 1987 Summer Program of the Center for the Turbulence Research, NASA-Ames and Stanford University*, pp. 237–251.

JOHANSSON, A. V., HER, A. V. & HARITONODIS, J. H. 1987 On the generation of high amplitude pressure peaks in turbulent boundary layers and spots. *J. Fluid Mech.* **175**, 119.

KIM, J. 1989 On the structure of pressure fluctuations in simulated turbulent channel flow. *J. Fluid Mech.* **205**, 421.

KIM, J. & MOIN, P. 1986 Flow structures responsible for the bursting process. *Bull. Am. Phys. Soc.* **31**, 1716.

KIM, J., MOIN, P. & MOSER, R. 1987 Turbulence statistics in fully developed channel flow at low Reynolds number. *J. Fluid Mech.* **177**, 133.

KLINE, S. J., REYNOLDS, W. C., SCHRAUB, F. A. & RUNSTADLER, P. W. 1967 The structure of turbulent boundary layers. *J. Fluid Mech.* **30**, 741.

KRAVCHENKO, A. G., CHOI, H. & MOIN, P. 1993 On the relation of near-wall streamwise vortices to wall skin friction in turbulent boundary layers. *Phys. Fluids* A **5**, 3307.

KUHN, G. D., MOIN, P., KIM, J. & FERZIGER, J. H. 1984 Turbulent flow in a channel with a wall with progressive waves. *Proceedings ASME Symp. on Laminar Turbulent Boundary Layers: Control, Modification and Marine Applications, New Orleans.*

LAURIEN, E. & KLEISER, L. 1989 Numerical simulation of boundary-layer transition and transition control. *J. Fluid Mech.* **199**, 403.

LUMLEY, J. L. 1973 Drag reduction in turbulent flow by polymer additives. *J. Polymer Sci.* D: *Macromol. Rev.* **7**, 263.

METCALFE, R. W., RUTLAND, C. J, DUNCAN, J. H. & RILEY, J. J. 1986 Numerical simulation of active stabilization of laminer boundary layers. *AIAA J.* **24**, 1494.

MOIN, P. 1987 Analysis of turbulence data generated by numerical simulations. *AIAA Paper* 87–0194.

MOIN, P., KIM, J. & CHOI, H. 1989 On the active control of wall-bounded turbulent flows. *AIAA Paper* 89–0960.

NARASIMHA, R. 1983 The turbulence problem: a survey. *J. Indian Inst. Sci.* **64** (A), 1.

NGUYEN, V. D., SAVILL, A. M. & WESTPHAL, R. V. 1987 Skin friction measurements following manipulation of a turbulent boundary layer. *AIAA J.* **25**, 498.

ORLANDI, P. 1990 Vortex dipole rebound from a wall. *Phys. Fluids* A **2**, 1429.

ROBINSON, S. K. 1991 Coherent motions in the turbulent boundary layer. *A. Rev. Fluid Mech.* **23**, 601.

WALLACE, J. M., ECKELMANN, H. & BRODKEY, R. S. 1972 The wall region in turbulent shear flow. *J. Fluid Mech.* **54**, 39.

WALSH, M. J. 1982 Turbulent boundary layer drag reduction using riblets. *AIAA Paper* 82-0169.

WHITE, F. M. 1974 *Viscous Fluid Flow*. McGraw-Hill.

WILLMARTH, W. W. & LU, S. S. 1972 Structure of the Reynolds stress near the wall. *J. Fluid Mech* **55**, 65.